Bioorganic & Medicinal Chemistry Letters 21 (2011) 4784–4787

Contents lists available at ScienceDirect

Bioorganic & Medicinal Chemistry Letters

journal homepage: www.elsevier.com/locate/bmcl

3-(3-Phenoxybenzyl)amino-β-carboline: A novel antitumor drug targeting α-tubulin

Reiko Ikeda [a,b], Masaki Kurosawa [a], Takazumi Okabayashi [a], Ayako Takei [a], Masamichi Yoshiwara [a], Tadashi Kumakura [a], Norio Sakai [a], Osamu Funatsu [c], Akinori Morita [d], Masahiko Ikekita [c,d], Yumi Nakaike [a], Takeo Konakahara [a,b,e,*]

[a] Department of Pure and Applied Chemistry, Faculty of Science and Technology, Tokyo University of Science (RIKADAI), Noda, Chiba 278-8510, Japan
[b] Center for Technologies Against Cancer, Tokyo University of Science (RIKADAI), Noda, Chiba 278-8510, Japan
[c] Biome and Drug Research Center, Tokyo University of Science (RIKADAI), Noda, Chiba 278-8510, Japan
[d] Department of Applied Biological Science, Faculty of Science and Technology, Tokyo University of Science (RIKADAI), Noda, Chiba 278-8510, Japan
[e] Research Institute for Science and Technology, Tokyo University of Science (RIKADAI), Noda, Chiba 278-8510, Japan

ARTICLE INFO

Article history:
Received 18 March 2011
Revised 14 June 2011
Accepted 14 June 2011
Available online 22 June 2011

Keywords:
β-Carboline
α-Tubulin
Antitumor drug
Apoptosis

ABSTRACT

3-(3-Phenoxybenzyl)amino-β-carboline **2h** showed extremely-high activity; the IC_{50} value was 0.074 μM. To verify **2h**-induced cell death types, we observed the chromatin condensation, the DNA fragmentation and activated caspase-3 using Hoechst 33342, agarose electrophoresis and western blot, and suggesting **2h**-induced cell death type was apoptosis. Flow cytometry showed that **2h**-treated cell was induced SubG1 cell population after G2/M cell cycle arrest. In addition, using affinity chromatography and peptide mass fingerprinting, we found that interacting protein with this compound was α-tubulin protein.

Many anticancer drugs exert their cytotoxic effects by interfering with cell cycle progression via inhibition or activation of cell cycle regulators, inhibition of DNA replication, induction of DNA damage, or disruption of mitotic spindle formation.[1] In particular, since taxol was discovered, spindle microtubules have become a popular target for development of new anticancer drugs.[2,3] Antimicrotubule agents exert their cytotoxic effects during mitosis by interfering with the exchange of tubulin subunits between the microtubules and the free tubulin pool.[4] These drugs inhibit cell proliferation either by increasing microtubule polymerization, for example, taxol, or by promoting microtubule depolymerization, for example, the vinca alkaloids, and thus impede cell division and induce cell death at relatively high concentrations.[5] Many plant-derived products are used to combat malignant tumors. The chemotherapeutic drugs widely used in clinical oncology include anticancer compounds extracted from plants such as taxol and etoposide, or derived from plants alkaloids by simple chemical modification such as the camptothecin (CPT) derivatives topotecan and irinotecan.

β-Carboline has a planar tricyclic ring structure, and the derivatives are widely distributed in nature including in plants, marine life, human tissues, and body fluids.[6] Harman and norharman are very well known. Most of these β-carboline derivatives are endowed with antitumor, anticancer, or intercalating properties. Some of these molecules are benzodiazepine receptors, and their high DNA binding affinity is thought to be partially responsible for their pharmacological activity.[7–10] The interest in clinical application of β-carbolines is based on the physiological effects of these compounds, such as inhibition of cyclin-dependent kinase (CDK),[11] IkappaB kinase (IKK)[12] and topoisomerase I.[9] However, an optimal structure of β-carboline derivatives remains not to be identified. Therefore, in the present study, we synthesized a variety of β-carboline derivatives and evaluated their biological activities.

To determine the cytotoxic effects of synthesized β-carboline derivatives on a human cervical cancer cell line (HeLa S-3), we used the 3-(4,5-dimethylthiazol-2-yl)-2,5-diphenyltetrazolium bromide (MTT) assay (Tables 1–3). Previously, we reported that 3-benzylamino-β-carboline has high-antitumor activity, with an IC_{50} value of 0.11 μM.[13] On the other hand, Boursereau et al. reported that 1-amino-β-carboline has significant anticancer and antiparasite activities.[14]

Therefore, 1-benzylamino-β-carboline derivatives **1a–n** were synthesized from benzaldehyde possessing a methyl, chloro, methoxy, phenoxy, or hydroxy group by reductive amination with 1-amino-β-carboline in moderate to good yields as shown in

* Corresponding author.
E-mail address: konaka@rs.noda.tus.ac.jp (T. Konakahara).

0960-894X/$ - see front matter © 2011 Elsevier Ltd. All rights reserved.
doi:10.1016/j.bmcl.2011.06.061

Table 1
Yields and antitumor activity of 1-benzylamino-β-carbolines in HeLa S-3 cells

Compds	R^2	R^3	R^4	Yield (%)	IC_{50}[a] (μM)
1a	H	H	H	66	24 ± 1
1b	Me	H	H	92	13 ± 1
1c	H	Me	H	74	22 ± 6
1d	H	H	Me	68	26 ± 2
1e	Cl	H	H	68	19 ± 2
1f	H	Cl	H	93	20 ± 4
1g	H	H	Cl	67	18 ± 3
1h	H	Cl	Cl	69	20 ± 1
1i	OMe	H	H	75	15 ± 1
1j	H	OMe	H	77	24 ± 1
1k	H	H	OMe	54	22 ± 2
1l	H	OPh	H	84	2.3 ± 0.1
1m	H	H	OPh	90	15 ± 2
1n	OH	H	H	75	19 ± 1

[a] Drug toxicity was determined by 3-(4,5-Dimethylthiazol-2-yl)-2,5-diphenyltetrazolium bromide (MTT) assay (see Materials and methods). IC50 is drug concentration inhibited the 50% cell growth. Data represent the mean ± S.D. from four independent experiments performed in triplicate experiments.

Table 2
Yields and antitumor activity of 3-benzylamino-β-carbolines in HeLa S-3 cells

Compds	R^2	R^3	R^4	Yield (%)	IC_{50}[a] (μM)
2a	H	H	H	81	0.11 ± 0.01
2b	Me	H	H	82	0.30 ± 0.04
2c	H	Me	H	81	0.21 ± 0.01
2d	H	H	Me	73	6.2 ± 0.2
2e	OH	H	H	79	28 ± 2
2f	H	OH	H	80	0.92 ± 0.10
2g	H	H	OH	79	1.7 ± 0.2
2h	H	OPh	H	85	0.074 ± 0.007
2i	H	H	OPh	73	1.2 ± 0.1
2j	H	OBn	H	69	0.38 ± 0.05
2k	Cl	H	H	89	1.0 ± 0.1
2l	H	Cl	H	89	0.83 ± 0.05
2m	H	H	Cl	74	6.1 ± 1.1
2n	NO_2	H	H	71	14 ± 1
2o	H	NO_2	H	82	>30
2p	CF_3	H	H	75	6.7 ± 0.7
2q	H	CF_3	H	88	3.1 ± 0.4
2r	H	H	CF_3	74	47 ± 10
2s	Ph	H	H	88	3.0 ± 0.4
2t	H	H	Ph	74	>30

[a] Drug toxicity was determined by 3-(4,5-Dimethylthiazol-2-yl)-2,5-diphenyltetrazolium bromide (MTT) assay (see Materials and methods). IC50 is drug concentration inhibited the 50% cell growth. Data represent the mean ± S.D. from four independent experiments performed in triplicate experiments.

Table 3
Antitumor activity of multi-substituted 3-benzylamino-β-carbolines in HeLa S-3 cells

Compds	R^2	R^3	R^4	R^5	R^6	Yield (%)	IC_{50}[a] (μM)
3a	MeO	H	H	H	H	86	0.80 ± 0.06
3b	H	MeO	H	H	H	73	0.79 ± 0.04
3c	H	H	MeO	H	H	82	20 ± 4
3d	MeO	MeO	H	H	H	63	3.2 ± 0.4
3e	MeO	H	MeO	H	H	78	4.8 ± 0.3
3f	MeO	H	H	MeO	H	72	6.1 ± 0.6
3g	MeO	H	H	H	MeO	69	2.3 ± 0.2
3h	H	MeO	MeO	H	H	74	>100
3i	H	MeO	H	MeO	H	73	1.7 ± 0.4
3j	MeO	MeO	MeO	H	H	63	4.0 ± 0.8
3k	H	MeO	MeO	MeO	H	66	0.22 ± 0.03

[a] Drug toxicity was determined by 3-(4,5-Dimethylthiazol-2-yl)-2,5-diphenyltetrazolium bromide (MTT) assay (see Materials and methods). IC50 is drug concentration inhibited the 50% cell growth. Data represent the mean ± S.D. from four independent experiments performed in triplicate experiments.

Scheme 1 and Table 1, according to a usual method (see Supplementary data).

Next, we evaluated the cytotoxicity on a human cervical cancer cell line, HeLa S-3, of compounds **1b–n** by MTT method (Table 1).

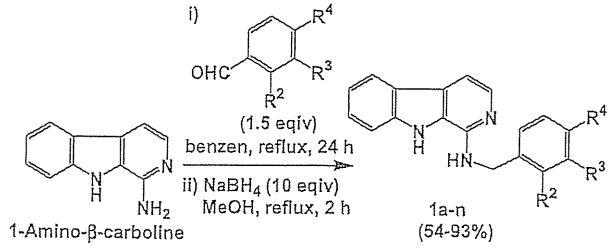

Scheme 1.

The compound **1l** with an OPh group at R^3 showed the highest antitumor activity; the IC_{50} value of **1l** was 2.3 μM. However, the activity of **1l** was lower than that of 3-benzylamino-β-carboline (**2a**), which had an IC_{50} value of 0.11 μM (Table 2). These results suggest that the optimal position for introduction of the benzylamino group is the 3-position of β-carboline nucleolus. Based on this result, we started to optimize the structure of 3-benzylamino-β-carboline to obtain the highest antitumor activity.

3-Benzylamino-β-carboline derivatives **2a–t** were analogously synthesized from 3-amino-β-carboline and benzaldehydes with a methyl, hydroxyl, phenoxy, benzyloxy, chloro, nitro, trifluoromethyl, or phenyl group at R^2–R^4 (Scheme 2). Yields are summarized in Table 2.

Cytotoxicity of **2a–t** was evaluated using the MTT assay (Table 2). In general, compounds substituted at R^2 and R^3 showed relatively high antitumor activity. In addition, the antitumor activity of the compounds substitutes at R^3 was higher than that of compounds substituted at R^4. In other words, substitution at the R^4 position reduced the antitumor activity. It was notable that **2h** which has a phenoxy group, had the highest-activity among the compounds **2a–t**; the IC_{50} value of **2h** is 0.074 μM. However, the introduction of a NO_2 or CF_3 group significantly reduced the antitumor activity.

Subsequently, in order to determine the influence of poly-substitution on antitumor activity, we synthesized 3-(dimethoxybenyl)amino-, and 3-(trimethoxybenyl)amino-β-carboline derivatives **3d–k** by the same method used in the synthesis of **2** as shown in Scheme 3 (see Supplementary data) in moderate to good yields, and evaluated the antitumor activity of these compounds (Table 3). Compared with di-substituted compounds, the tri-substituted derivatives were obtained in slightly lower yield due to steric hindrance. In each case, most of the starting material was recovered together with the desired product. Our efforts to improve the yield of poly-substituted product were unsuccessful. In addition, use of excess aldehyde caused the formation of bis-benzylated compounds.

The 2-, and 3-methoxy derivatives **3a,b** have similarly high antitumor activity, with the IC_{50} values of 0.80 and 0.79 μM, respectively. However, 4-methoxy derivative **3c** shows significantly reduced antitumor activity. These results suggest that the optimal position for monomethoxy-substitution was either the position 2 or 3. To determine the synergistic effect of dimethoxy-substitution on the antitumor activity, the 2,3-, 2,4-, 2,5-, and

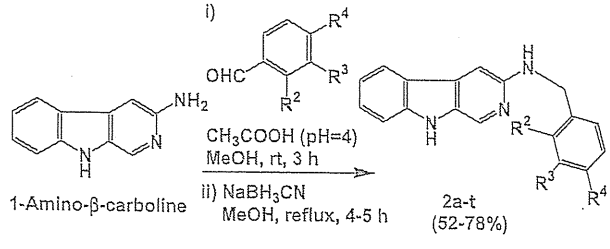

Scheme 2.

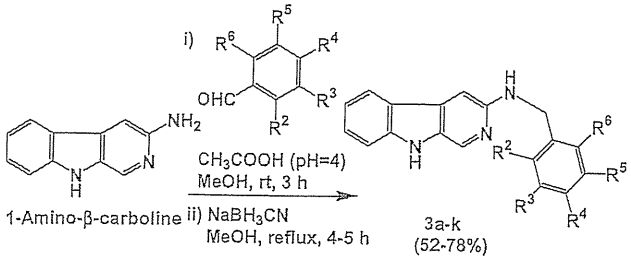

Scheme 3.

2,6-dimethoxy-substituted derivatives **3d–g** were synthesized in 63%, 78%, 72%, and 69% yields, respectively (Table 3). The antitumor activities of **3a,b** are very high. However, the antitumor activities of **3d–g** are lower than those of **3a,b**. Among these compounds, introduction of the 2nd methoxy group at the position 3, 4, 5, or 6 of **3a** slightly decreased the antitumor activity. The 4-methoxy group greatly decreased the antitumor activity of the corresponding compound (see **3c** in Table 3). Especially, introduction of the 2nd 4-methoxy group to **3b** strongly decreases the antitumor activity of the β-carboline derivative **3h**. Although the reason is not clear, 3-(3,4,5-trimethoxybenzyl)amino-β-carboline (**3k**) surprisingly shows the highest antitumor activity among the compounds **3a–k**, regardless of its 4-methoxy group; the IC_{50} value of **3k** is 0.22 μM, as shown in Table 3.

Next, we investigated the type of cell death induced. Both chromatin condensation and fragmented nuclei are the classic characteristics of apoptosis. Hoechst 33342 staining showed significant morphological changes in the nuclear chromatin. After treatment of HeLa S-3 cells 0, 150, 300, 1000 nM of **2h**, we observed the nuclear chromatin (Fig. 1). Compared with **2h**-treated cells, untreated cells exhibited less intense nuclear staining. However, a large proportion of **2h**-treated cells exhibited fragmented nuclei.

To verify that cell death occurred via apoptosis, a DNA fragmentation assay was performed. DNA fragmentation is a well known biochemical index of cell apoptosis. After exposure to **2h** for 48 h, the genomic DNA was extracted and analyzed by electrophoresis (Fig. 2). DNA fragmentation was detectable in the cells treated with **2h** (150–1000 nM). Together with fluorescence microscopy analysis, these observations demonstrated that **2h** caused apoptotic cell death.

Caspase-3 is well known as the execution factor of apoptosis. After determining that **2h** induced chromatin condensation and DNA fragmentation, we further investigated the activation of caspase-3 in **2h**-treated cells. As shown in Figure 3, activated caspase-3 was readily detected in cells treated with **2h** for more than 12 h, and it enhanced with the time-dependent. These observations are closely connected with results of the chromatin condensation and DNA fragmentation, suggesting that **2h** induced apoptosis.

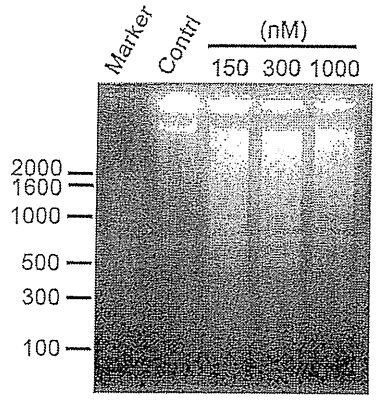

Figure 2. Effect of 2h on apoptosis induction in HeLa S-3 cells. Cells were treated with **2h** for 48 h. DNA fragmentation was detected by electrophoresis on a 2% agarose gel. Marker; 100 bp ladder.

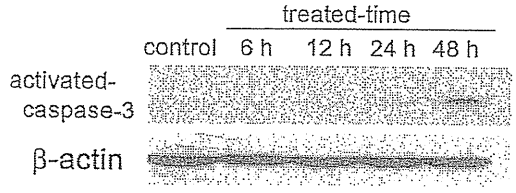

Figure 3. Western blot analysis of activated caspase-3 in HeLa S-3 cells. Cells were treated with **2h** for 6, 12, 24 or 48 h. Control, non-treated cell extract; β-actin was used as internal control.

To examine the effects on cell cycle progression, the cells were exposed to 150 nM of **2h** for 12, 24, 36, or 48 h. After treating for 12 h, the percentage of average G_2/M population at the control cells was 65.92% (see Table 4). For 24 h, this population shifted from G_2/M phase to the mean apoptotic population sub-G_1 phase. These results suggest that **2h** induces apoptosis through G_2/M cells cycle arrest.

Affinity chromatography, which is based on a highly specific biological interaction, such as between antigen and antibody, enzyme and substrate, or receptor and ligand, is used to separate biochemical mixture. In the present study, we sought to identify the

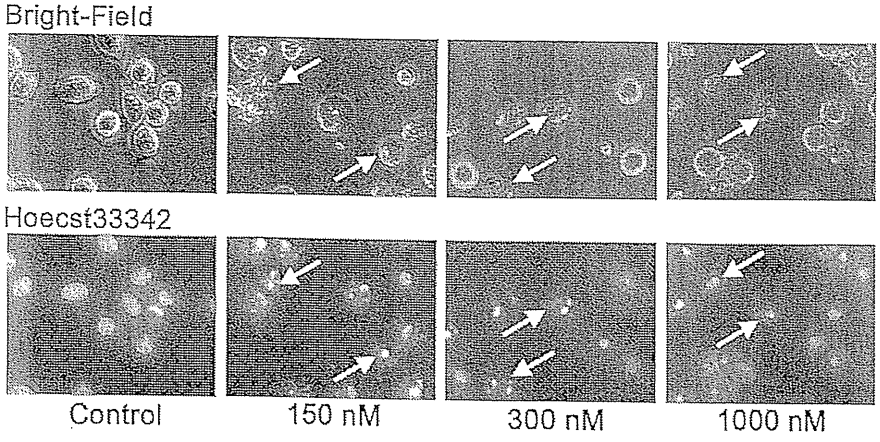

Figure 1. HeLa S-3 cells were treated with 2h for 48 h. Apoptosis was detected by Hoechst 33342 staining.

Table 4
Effect of **2h** on the distribution of cell-cycle phase in HeLa S-3

Treatment time (h)	SubG$_1$ (%)	G$_1$ (%)	S (%)	G$_2$/M (%)
Control	1.51	56.42	19.62	22.45
12	9.72	8.40	15.38	65.92
24	32.74	21.18	15.93	30.01
36	43.51	18.97	15.62	19.19
48	50.14	18.38	20.16	9.52

HeLa S-3 cells were incubated in the absence (control) or presence of **2h** for 12, 24, 36, or 48 h. Then, the cells were fixed and stained with propidium iodide to analyze DNA content by flow cytometer.

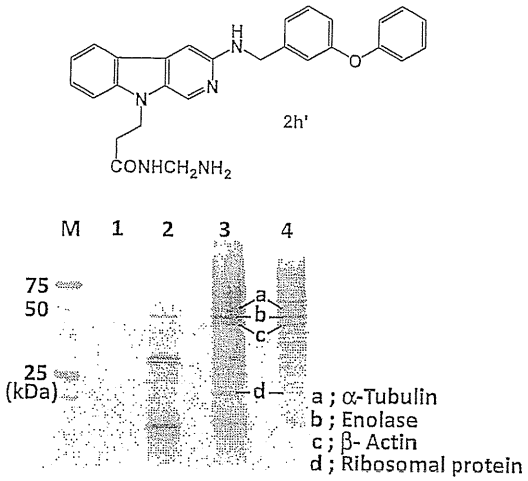

Figure 4. SDS–PAGE analysis of the proteins enriched by affinity chromatography. The ligand (**2h**) was introduced using amino-linker (upper panel). M, size-marker; (1) using NHS-activated sepharose 4 Fast Flow as negative control; (2) solubilized fraction of interacting protein; (3) insolubilized fraction of interacting protein; (4) whole cell lysate.

proteins that interact with **2h**, because it showed the highest antitumor-activity and induced apoptosis. The compound **2h** was used as the ligand on an affinity column, and was immobilized using an amino-linker (Fig. 4, upper panel). The proteins that interacted with the probe **2h'** were separated by electrophoresis, and subsequently identified using matrix-assisted laser desorption ionization/time of flight-mass spectrometry (MALDI/TOF-MS) (Fig. 4, lower panel, a–d). The proteins shown in a–d were α-tubulin, enolase, β-actin, ribosomal protein, respectively.

Many anticancer drugs are cytotoxic because they interfere with cell cycle progression by inhibition of activation of cell cycle regulation, inhibition of DNA replication, induction of DNA damage, or disruption of mitotic spindle formation.[1] In particular, since taxol was discovered, spindle microtubules have become a popular target for the development of new anticancer drugs.[2,3] These drugs inhibit cell proliferation either by increasing microtubule polymerization, for example, taxol, or by promoting microtubules depolymerization, for example, the vinca alkaloids, thus impeding cell division and inducing cell death at relatively high concentrations.[5] These reports indicate that a delay in progression through mitosis by the induction of aberrant spindle formation might be another mechanism by which anticancer drugs alter cancer cell growth.

In the present study, results of affinity chromatography and peptide mass fingerprinting showed that the protein with the strongest interaction was enolase (Fig. 4). However, inhibition of enolase was probably caused by blockade of the glycolytic system, such as inhibition of the citric acid cycle or the electron transfer system. During preparation for cell division under conditions of energy deficiency, a variety of cell cycle regulators might interfere with the onset of the M phase. Therefore, it does not stand to reason that the cell cycle progressed through the anaphase stage of cell division after DNA replication. Based on the results of the present study, it is reasonable to suggest that α-tubulin might interacting with **2h**. In addition, the flow cytometric analysis demonstrated G$_2$/M-phase arrest of the cell cycle with **2h**. Many microtubule-interfering agents bind to β-tubulin and induce arrest of cell division. Among them, colchicines, vinblastine and taxol have played major roles in practical uses as well as in biochemical studies of microtubules functions. Each of these compounds binds to β-tubulin, however, the protein that interacted with **2h** was α-tubulin. Therefore, **2h** appears to have a different mechanism of action compared with the colchicines, vinblastine and taxol.

The function of α-tubulin in the apoptosis pathway is unclear, and antitumor drugs that are currently in use do not target this protein. For these reasons, the consequences of **2h** effects on α-tubulin remain unclear. Characterization of the relationship between α-tubulin and apoptosis requires identification of molecular/biological mechanisms.

Acknowledgments

This work was partially supported by a Grant-in-Aid for Scientific Research from MEXT, a matching fund subsidy from MEXT 2004–2006 (No. 16550148); a grant for the 'High-Tech Research Center' Project for Private Universities, a matching fund subsidy from MEXT, 2000–2004 and 2005–2007; a Grant from the Japan Private School Promotion Foundation (2008–2009); a Grant-in-Aid for Scientific Research form MEXT, a matching fund subsidy from MEXT 2009–2011 (No. 21590025); and a grant for the Development of strategic Research Center in Private Universities supported by MEXT, Center for Technologies against Cancer (CTC), 2009–2013. We thank Sanae Takasugi, Masaki Takizawa, Takuya Akahane and Taro Nittono (Department of Pure and Applied Chemistry, Faculty of Science and Technology, Tokyo University of Science (RIKADAI)) for experimental work in the synthesis of **3d–k** and MTT assay of **3h–i**.

Supplementary data

Supplementary data associated with this article can be found, in the online version, at doi:10.1016/j.bmcl.2011.06.061.

References and notes

1. Stewart, Z. A.; Westfall, M. D.; Pietenpol, J. A. *Trends Pharmacol. Sci.* 2003, *24*, 139.
2. Gibbs, J. B. *Science* 2000, *287*, 1969.
3. Jordan, M. A. *Curr. Med. Chem. Anti-Cancer Agents* 2002, *2*, 1.
4. Wood, K. W.; Cornwell, W. D.; Jackson, J. R. *Curr. Opin. Pharmacol.* 2001, *1*, 370.
5. Dumontet, C.; Sikic, V. I. *J. Clin. Oncol.* 1999, *17*, 1061.
6. Cao, R.; Peng, W.; Wang, Z.; Xu, A. *Curr. Med. Chem.* 2007, *14*, 479.
7. Hayashi, K.; Nagao, M.; Sugimura, T. *Nucleic Acids Res.* 1977, *4*, 3679.
8. Ishida, J.; Wang, H. K.; Bastow, K. F.; Hu, C. Q.; Lee, K. H. *Bioorg. Med. Chem. Lett.* 1999, *9*, 3319.
9. Cao, R.; Peng, W.; Chen, H.; Ma, Y.; Liu, X.; Hou, X.; Guan, H.; Xu, A. *Biochem. Biophys. Res. Commun.* 2005, *338*, 1557.
10. Zhao, T. J.; Rosenberg, H. C.; Chiu, T. H. *Eur. J. Pharmacol.* 1996, *306*, 61.
11. García, M. D.; Wilson, A. J.; Emmerson, D. P.; Jenkins, P. R. *Org. Biomol. Chem.* 2006, *4*, 4478.
12. Castro, A. C.; Dang, L. C.; Soucy, F. S.; Grenier, L. *Bioorg. Med. Chem. Lett.* 2003, *13*, 2419.
13. Konakahara, T.; Iida, T.; Iwaki, T.; Kumagai, M.; Sakai, N. JP2006321753.
14. Yohan, B.; Iain, C. *Bioorg. Med. Chem. Lett.* 2004, *14*, 5841.

Bioorganic & Medicinal Chemistry 19 (2011) 4162–4172

Contents lists available at ScienceDirect

Bioorganic & Medicinal Chemistry

journal homepage: www.elsevier.com/locate/bmc

Transformation of thiols to disulfides by epolactaene and its derivatives

Kouji Kuramochi [a,*], Takashi Sunoki [b], Kazunori Tsubaki [a], Yoshiyuki Mizushina [c,d], Kengo Sakaguchi [e], Fumio Sugawara [e], Masahiko Ikekita [e], Susumu Kobayashi [b]

[a] Graduate School of Life and Environmental Sciences, Kyoto Prefectural University, Kyoto 606-8522, Japan
[b] Faculty of Pharmaceutical Sciences, Tokyo University of Science, 2641 Yamazaki, Noda, Chiba 278-8510, Japan
[c] Laboratory of Food & Nutritional Science, Department of Nutritional Science, Kobe-Gakuin University, Nishi-ku, Kobe, Hyogo 651-2180, Japan
[d] Cooperative Research Center of Life Sciences, Kobe-Gakuin University, Chuo-ku, Kobe, Hyogo 650-8586, Japan
[e] Department of Applied Biological Science, Faculty of Science and Technology, Tokyo University of Science, 2641 Yamazaki, Noda, Chiba 278-8510, Japan

ARTICLE INFO

Article history:
Received 11 May 2011
Revised 2 June 2011
Accepted 3 June 2011
Available online 13 June 2011

Keywords:
Epolactaene
γ-Lactam
Epoxide
Thiol
Disulfide
Thiolysis

ABSTRACT

In this paper we report a disulfide formation of thiols induced by epolactaene and its derivatives. We previously reported the disulfide formation of *N*-acetylcysteine methyl ester by epolactaene in a 1:1 MeOH/0.5 M $NaHCO_3$ aq solution. The present studies reveal that the disulfide formation proceeds under mild conditions such as in PBS at pH 7.3, suggesting that epolactaene may induce disulfide formation of cellular thiols. This compound induces the disulfide formation of several thiols in a 1:1 MeOH/0.5 M $NaHCO_3$ aq solution at room temperature. Moreover, our results show that the acyl side-chain of epolactaene greatly influences the products of the reaction. We analyzed the reaction mechanism by using thiolysis products of epolactaene derivatives and propose a new reaction mechanism.

1. Introduction

Disulfide bonds play an important role in stabilizing protein structures and mediating the biological functions of proteins.[1–3] Reversible disulfide bond formation and the associated conformation changes are likely to play an important role in cellular redox regulation.[4–6] In eukaryotic cells, disulfide formation usually occurs in the lumen of the endoplasmic reticulum (ER) and the intermembrane space of mitochondria, but not in the cytosol.[7] The disulfide formation can proceed spontaneously in the presence of sufficient oxidant.[8,9] Recent evidence indicates that reactive oxygen species can act as signaling molecules by promoting the formation of disulfide bonds within or between select redox-sensitive proteins.[10]

Epolactaene (**1a**), a microbial metabolite isolated from *Penicillium* sp., has several attractive biological activities such as promotion of neurite outgrowth and induction of G0/G1 cell cycle arrest in a human neuroblastoma cell line SH-SY5Y,[11–14] an apoptosis-inducing activity in a human leukemia B cell line BALL-1,[15,16] inhibition of mammalian DNA polymerase and DNA topoisomerase activities,[17,18] and an anti-inflammatory activity on TPA (12-*O*-tetradecanoylphorbol 13-acetate)-induced inflammation.[19] We established an efficient synthesis of epolactaene via an oxiranyl anion derived from the α,β-epoxy-γ-lactone.[20–23] Using this synthetic methodology, we prepared several epolactaene derivatives to investigate the structure–activity relationship as well as its biological mechanism of action and to further examine potential new biological activities. In the course of our studies on the chemistry and biology of epolactaene and its derivatives, we found that epolactaene (**1a**) induce the disulfide formation of *N*-acetylcysteine methyl ester (**2**) (Scheme 1).[24] Treatment of **1a** and **2** (1.5 mol equiv) in a 1:1 MeOH/0.5 M $NaHCO_3$ aq solution gave the disulfide **3** in 77% yield and the carboxylic acid **4a** in 72% yield. This disulfide bond formation is unique in the following respect. (i) Epolactaene (**1a**) acts as an oxidant to induce the disulfide formation. (ii) This reaction is mechanistically interesting because the side-chain ketone of **1a** is converted into the corresponding carboxylic acid **4a** under mildly basic conditions. (iii) Epolactaene and its derivative might induce the disulfide formation of specific cellular thiols, which may account for their biological activities.[25–29]

In this paper, we report the disulfide formation of epolactaene and its derivatives.

2. Results

2.1. Reaction of epolactaene with thiols

We first examined the reaction of epolactaene (**1a**) and *N*-acetylcysteine methyl ester (**2**; 2.0–2.3 mol equiv) in various media

* Corresponding author. Tel./fax: +81 75 703 5603.
E-mail address: kuramoch@kpu.ac.jp (K. Kuramochi).

0968-0896/$ - see front matter © 2011 Elsevier Ltd. All rights reserved.
doi:10.1016/j.bmc.2011.06.015

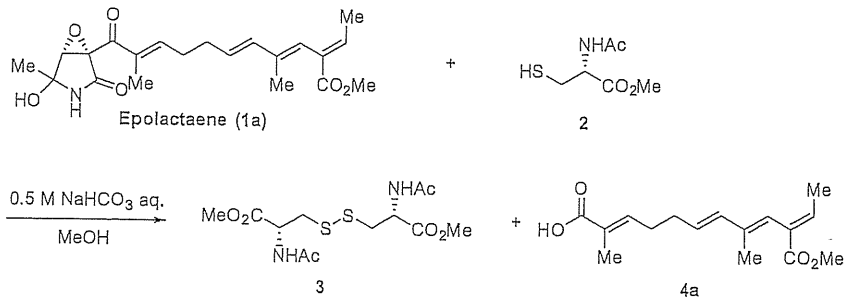

Scheme 1. Reaction of epolactaene (1a) with *N*-acetylcysteine methyl ester (2).

(Table 1). Treatment of **1a** and **2** in a 1:1 MeOH/0.5 M $NaHCO_3$ aq solution gave the disulfide **3** in 75% yield and the carboxylic acid **4a** in 68% yield (entry 1). This reaction proceeded smoothly and was complete in 10 min at room temperature. The reaction of **1a** and **2** with solid $NaHCO_3$ in unpurified MeOH gave **3** in 55% yield and **4a** in 33% yield (entry 2). The reaction was slow and the yield of **3** was moderate. In this reaction the methyl ester of **4a** was not obtained at all, indicating that water present as a contaminant in the MeOH was involved in the transformation of **1a** into **4a**. Thus, it was reasoned that water might be implicated in the reaction.[30,31] Indeed, disulfide formation did not proceed in absolute MeOH, but was observed in water (see entries 3 and 4). The reaction in water was slow; after 24 h, the disulfide **3** was obtained in 25% yield and the starting thiol **2** was recovered in 72% yield. We next examined the effect of pH on the disulfide formation of **2** induced by **1a** (entries 5–7). The reaction of **1a** and **2** in 0.2 M phosphate buffer at pH 6.0 for 24 h gave **3** in 49% yield and recovered **2** in 39% yield. By contrast, reactions carried out at pH 7.0 and 8.0 were complete within 24 h, in each case affording **3** in good yield. The low solubility of **1a** and **2** in water or buffer is one of the reasons why the reaction proceeds slowly. However, the reaction in phosphate buffer at pH 7.0 was complete within 24 h, but not in water. This result can be accounted for by the decrease in pH of the reaction solution due to the production of the carboxylic **4a**. The disulfide formation also proceeded in phosphate buffered saline at pH 7.3 (entry 8), suggesting that **1a** induces intramolecular or intermolecular disulfide bond formation in cells.

We next examined the reaction of **1a** with various thiols (Table 2). The reaction was performed using a 1:2.2 mole ratio of **1a** and thiol in a 1:1 MeOH/0.5 M $NaHCO_3$ aq solution at room temperature. Both aromatic and primary thiols were converted to the corresponding disulfides in good yield (entries 1–4). However, the reaction of **1a** and *tert*-dodecyl mercaptan did not proceed, and both reactants were recovered (entry 5). The bulky thiols, such as tertiary thiols, do not react with **1a** presumably due to steric hindrance.

2.2. Reaction of epolactaene derivatives with thiols

We examined the reaction of epolactaene (**1a**) and its derivatives (**1b–d**) with 1.2–2.0 mol equiv of *N*-acetylcysteine methyl ester (**2**) (Table 3). Treatment of **1a** with **2** gave the disulfide **3** in 63%

Table 1
Disulfide formation of **2** induced by epolactaene (**1a**)

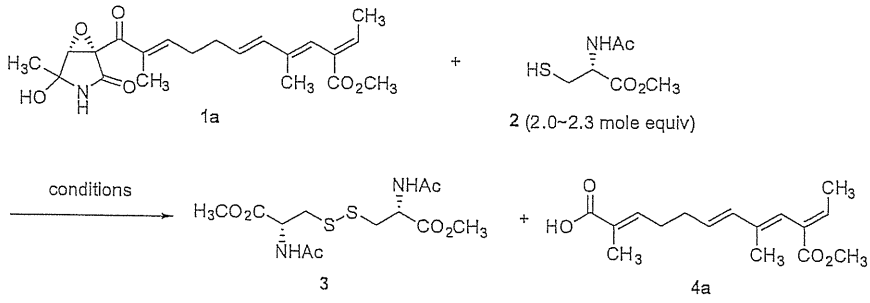

Entry	Conditions	Yield (%)	
		3[a]	4a[b]
1	MeOH:0.5 M $NaHCO_3$ aq = 1:1, 10 min	75 (88)	68
2	MeOH + $NaHCO_3$ (10 equiv), 6 h	55 (58)	33
3	MeOH, 24 h	No reaction	
4[c]	H_2O, 24 h	25 (27)	—
5[d]	Phosphate buffer (pH 6.0), 24 h	49 (52)	—
6	Phosphate buffer (pH 7.0), 24 h	82 (83)	47
7	Phosphate buffer (pH 8.0), 24 h	73 (76)	38
8	PBS (pH 7.3), 24 h	77 (81)	42

[a] Yields based on **2**. The yields in parentheses are those based on **1a**.
[b] Yields based on **1a**.
[c] 72% of **2** was recovered.
[d] 39% of **2** was recovered.

Table 2
Disulfide formation of various thiols induced by epolactaene (1a)

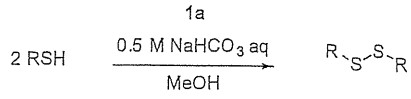

Entry[a]	Thiol	Time (h)	Yield[b] (%)
1	PhSH	0.5	89 (98)
2	2-Mercaptopyridine	4	86 (95)
3	$CH_3(CH_2)_5SH$	0.5	89 (98)
4	$CH_3(CH_2)_{11}SH$	0.5	73 (80)
5	$CH_3(CH_2)_8C(CH_3)_2SH$	24	No reaction

[a] The reaction was performed using a 1:2.2 mole ratio of 1a and thiol.
[b] Yields of disulfides based on thiols. The yields in parentheses are those based on 1a.

eld and the carboxylic acid **4a** in 60% yield (entry 1). As compared with entry 1 in Table 1, the yield of **3** and **4a** increased by using 2.2 mol equiv of **2**. In both reactions, only disulfide **3** and carboxylic acid **4a** were the products identified. Uniquely, reaction of Epo-C12 (**1b**) with 1.2 mol equiv of **2** gave the adduct **5b** as a sole product in 82% yield (entry 2).[24] However, reaction of **1b** with excess **2** (2.0 mol equiv) afforded the disulfide **3**, dodecanoic acid **4b** and **5b** in 64%, 42% and 13% yield, respectively (entry 3). Similarly, reaction of **1c**,[22] a C6-acyl derivative, with **2** (1.2 mol equiv) afforded **3**, hexanoic acid **4c** and the adduct **5c** in 48%, 29% and 25% yield, respectively (entry 4). However, reaction of **1d**, a phenyl derivative, with **2** gave **3** and benzoic acid **4d** in 56% and 58% yield, respectively (entry 5).

These results show that the acyl side-chain of **1** strongly influences the reaction between **1** and **2**. Both **1a** and **1d**, which have an unsaturated acyl side-chain, reacted with **2** to give the disulfide **3** and carboxylic acid **4**. Meanwhile, the adduct **5** was obtained by the reaction of **2** with **1b** or **1c**, which has a saturated acyl group.

We further investigated the effect of the amount of thiol on the reaction between **1b** and thiophenol (Table 4). Treatment of **1b** and thiophenol (1.0 mol equiv) gave diphenyl disulfide, **4b**, the adduct **6b** and γ-lactam **8-Ph** in 56%, 49%, 18% and 13% yield, respectively, accompanied by a trace amount of β-ketoamide **7b** (entry 1). The use of 2.0 mol equiv of thiophenol gave the disulfide, **4b** and **6b** in 85%, 20% and 9% yield, respectively (entry 2). In contrast to entry 1, compound **7b** and **8-Ph** were not obtained in entry 2. These results indicate that the amount of thiol influences the product of the reaction between **1b** and thiophenol.

2.3. Studies on the reaction mechanism

We previously proposed the mechanism of the disulfide formation of **2** induced by **1b** (Scheme 2).[24] The proposed reaction mechanism may involve the initial formation of the α-sulfanylketoamide (**5b**), followed by a retro-Claisen reaction to give carboxylic acid **4b**. Excess **2** then might react with methyl *N*-acetyl-*S*-(2-amino-2-oxoethyl)cysteinate **9**, the intermediate of the retro-Claisen reaction, yielding **3**.

To clarify that the retro-Claisen reaction actually occurs, compound **5b** was subjected to basic conditions in a 1:1 MeOH/0.5 M $NaHCO_3$ aq solution (Scheme 3A). However, the proposed retro-Claisen reaction did not proceed and only racemization at the cysteine moiety was observed. Next, to determine whether **5b** was the

Table 3
Reaction of epolactaene and its derivatives 1 (a–d) with 2

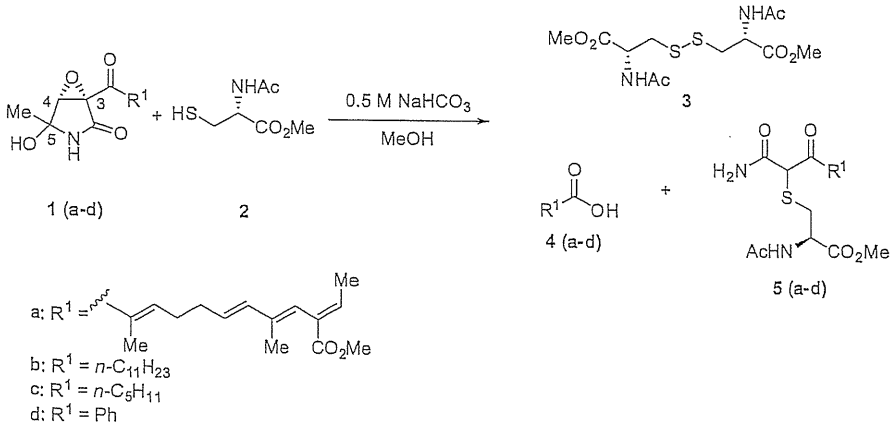

Entry	1	2 (mol equiv)	Yield (%)		
			3[a]	4[b]	5[b]
1	1a	1.2	63 (75)	4a: 60	–
2	1b	1.2	–	–	5b: 82
3	1b	2.0	64	4b: 42	5b: 13
4	1c	1.3	48 (62)	4c: 29	5c: 25
5	1d	1.2	56 (68)	4d: 58	–

[a] Yields based on 2. The yields in parentheses are those based on 1.
[b] Yields based on 1.

Table 4
Reaction of **1b** with thiophenol

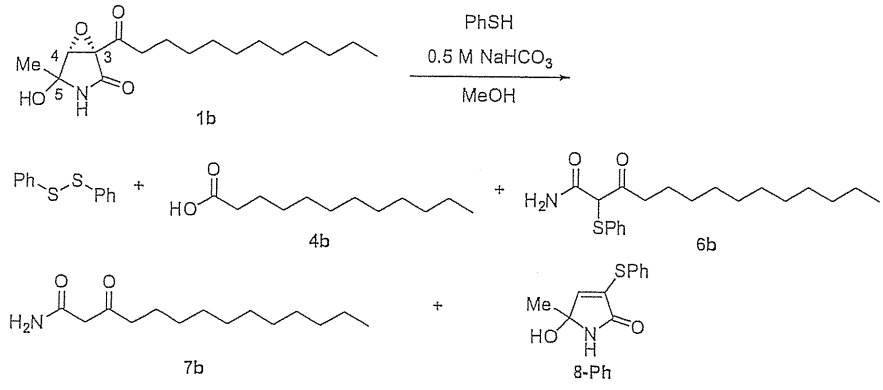

Entry	Thiol (mol equiv)	Time (h)	Disulfide	Yield (%)			
				4b	6b	7b	8-Ph
1	Thiophenol (1.0)	12	56	49	18	3	13
2	Thiophenol (2.0)	0.5	85	20	9	—	—

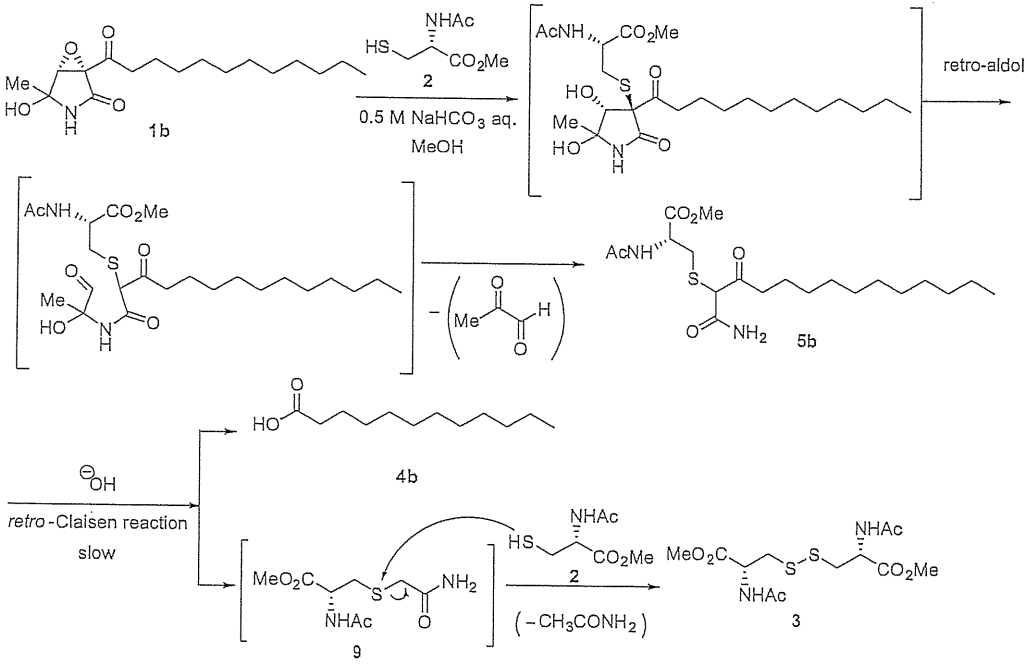

Scheme 2. The previously proposed mechanism.

intermediate for the disulfide formation of **2** by **1b**, we examined the reaction of **5b** with **2** (Scheme 3B). Treatment of **5b** with *N*-acetylcysteine methyl ester (**2**; 1.1 mol equiv) in a 1:1 MeOH/0.5 M $NaHCO_3$ aq solution for 16 h gave the disulfide **3** in 35% yield and the β-ketoamide **7b** in 17% yield, and the unreacted **5b** was recovered in 48% yield. Although the disulfide **3** was obtained in this reaction, no dodecanoic acid was generated. This result also indicates that the proposed retro-Claisen reaction did not proceed by the reaction of **5b** and **2** under the basic conditions. We also found that the reaction of **9** with **2** did not proceed (Scheme 4).

In addition, we checked whether the retro-Claisen reaction occurred during the reaction of **6b** with thiophenol (Scheme 5). Treatment of **6b** with thiophenol in a 1:1 MeOH/0.5 M $NaHCO_3$ aq solution for 21 h gave diphenyl disulfide and **7b** in 74% and 71% yield, respectively. Carboxylic acid **4b** was not obtained in this reaction, indicating that the retro-Claisen reaction did not proceed.

These results suggest that our proposed mechanism shown in Scheme 2 is probably incorrect and should be further examined. We considered that a retro-Claisen reaction of β-hydroxy-γ-lactam derivative **10** or **11** might occur under the basic conditions

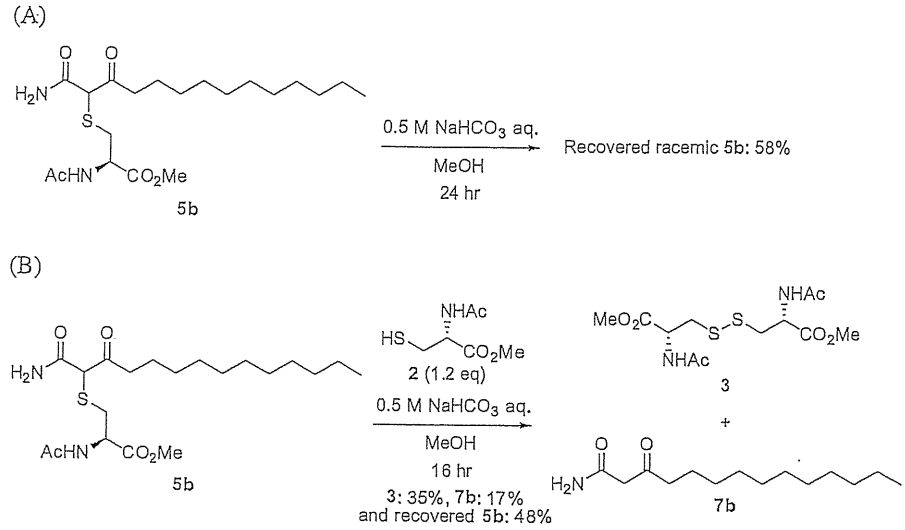

Scheme 3. Treatment of **5b** with a 1:1 MeOH/0.5 M $NaHCO_3$ aq solution in the absence (A) or presence (B) of **2**.

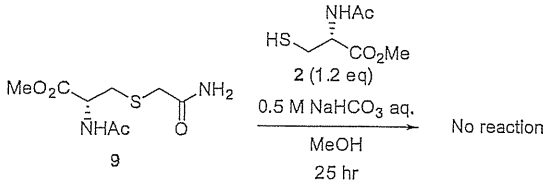

Scheme 4. Treatment of **9** with **2** in a 1:1 MeOH/0.5 M $NaHCO_3$ aq solution.

(Scheme 6).[32,33] We decided to prepare each compound by a coupling of methyl glyoxal and β-ketoamide derivatives.

Reaction of **6b** with methyl glyoxal in a 1:1 MeOH/0.5 M $NaHCO_3$ aq solution gave dodecanoic acid **4b** in quantitative yield (Scheme 7A). Although the desired β-hydroxy-γ-lactam derivative **10b** was not isolated, compound **4b** should be formed by retro-Claisen reaction of **10b** and **10b′**. We modified the reaction conditions to obtain β-hydroxy-γ-lactam derivatives (Scheme 7B). Treatment of **6b** and methyl glyoxal with sodium bicarbonate (3.2 equiv) in THF/MeOH/H_2O (4:1:1) gave **4b** in 86% yield and β-hydroxy-γ-lactam derivatives **12** as a 4:1 diastereomeric mixture at C-5, **13**, **14** and **15** in 36%, 17%, 5% and 4% yield, respectively. The relative stereochemistry of **14** and **15** were deduced by NOE experiments shown in Figure 1. Formation of these β-hydroxy-γ-lactams shows that the initial formation of **10b** and **10b′** followed by a retro-Claisen reaction certainly occurred in the reaction of **6b** and methyl glyoxal. These results (described in Scheme 7) demonstrate that a retro-Claisen reaction of α-sulfanyl-β-hydroxy-γ-lactam derivative **10** will proceed under the conditions of disulfide formation of thiols by **1**.

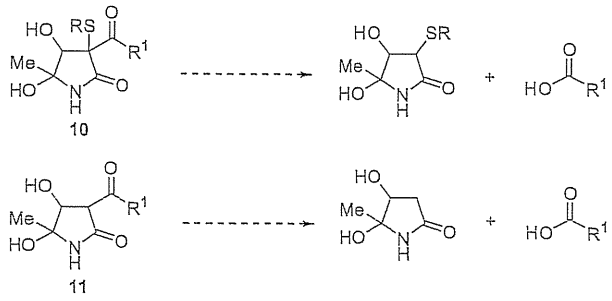

Scheme 6. Possible retro-Claisen reaction of **10** and **11**.

We assumed that the disulfide formation of thiophenol by **1** might proceed via compound **12**, **14** or **15**. However, treatment of **12** with thiophenol gave only **16** as a single diastereomer, and the disulfide formation was not observed in this reaction (Scheme 8). Treatment of **14** or **15** with thiophenol also afforded **16**. The relative stereochemistry of **16** (as well as **12**) was deduced by NOE correlations (Fig. 2). Furthermore, no reaction took place by treatment of **16** with thiophenol. Taken together, our results suggest that compounds **12**, **14** and **15** do not constitute key reaction intermediates for disulfide formation of thiophenol by **1**.

Next, we tried to prepare β-hydroxy-γ-lactam **11b** by a coupling of **7b** and methyl glyoxal.[34] We obtained α,β-unsaturated γ-lactam **17** by a coupling of **7b** with methyl glyoxal (1.1 equiv) in the presence of sodium bicarbonate (1.1 equiv) in THF/MeOH/H_2O (4:1:1) (Scheme 9). Compound **17** should be formed via **11b**. However, compounds **4b** and **11b** were not isolated in this reaction and only

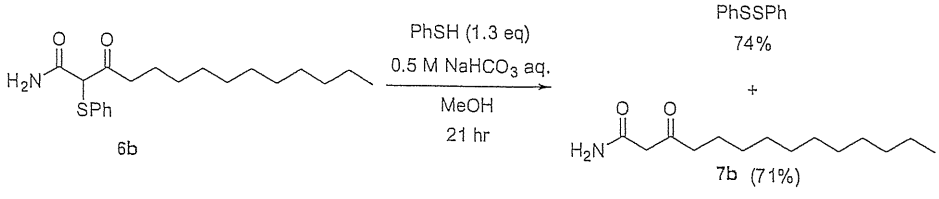

Scheme 5. Reaction of **6b** with thiophenol.

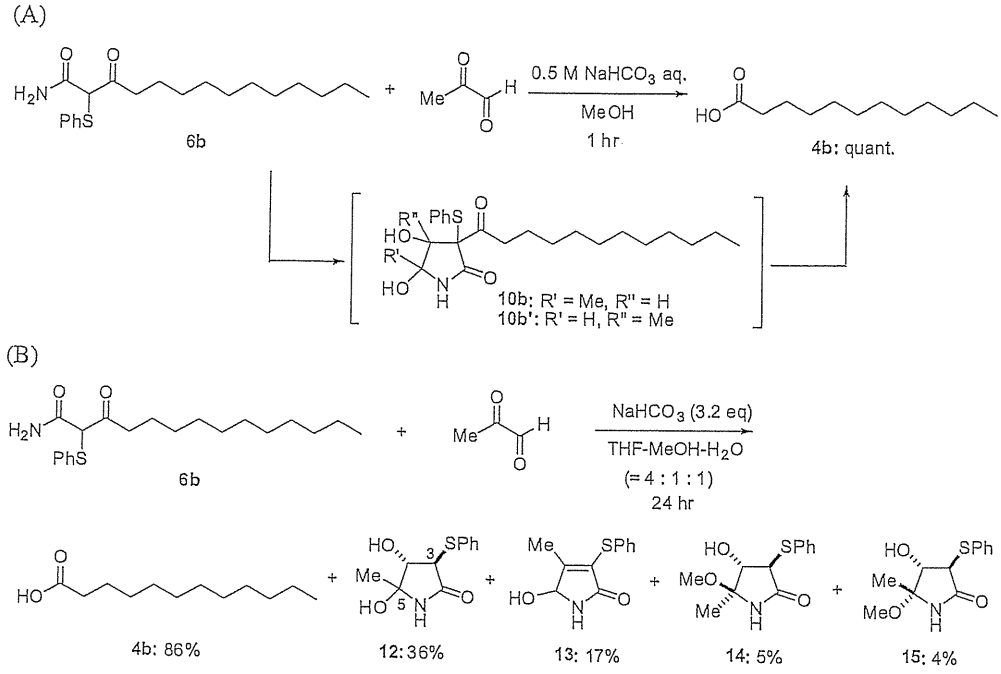

Scheme 7. Reaction of **6b** with methyl glyoxal in a 1:1 MeOH/0.5 M $NaHCO_3$ aq solution (A) and in 4:1:1 THF/MeOH/H_2O in the presence of $NaHCO_3$ (B).

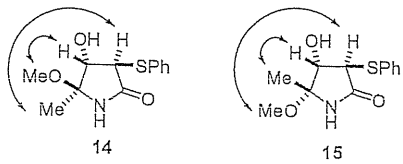

Figure 1. NOE correlations in compounds **14** and **15**.

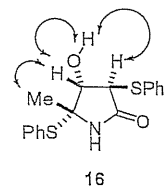

Figure 2. NOE correlations in compound **16**.

a couple of unidentified products were obtained. We attempted to conduct the reaction of **7b** with methyl glyoxal under various different conditions, but neither **11b** nor **4b** could be obtained (data not shown). Thus, we could not confirm whether the retro-Claisen reaction of **11b** actually proceeds.

However, treatment of **7d** with methyl glyoxal in a 1:1 MeOH/0.5 M $NaHCO_3$ aq solution gave benzoic acid **4d** in 21% yield, indicating that formation of **11d** or **11d'** followed by retro-Claisen reaction afforded **4d** (Scheme 10). This result leaves open the possibility that a retro-Claisen reaction of β-hydroxy-γ-lactam derivatives **11** may take place under the conditions of the disulfide formation of thiols by **1**.

3. Discussion

Epolactaene (**1a**) reacts with various thiols and induces disulfide formation. Given that disulfide formation is favored under basic conditions (Table 1) and that sterically bulky *tert*-dodecyl mercaptan does not react with **1a** (Table 2, entry 5), the reaction

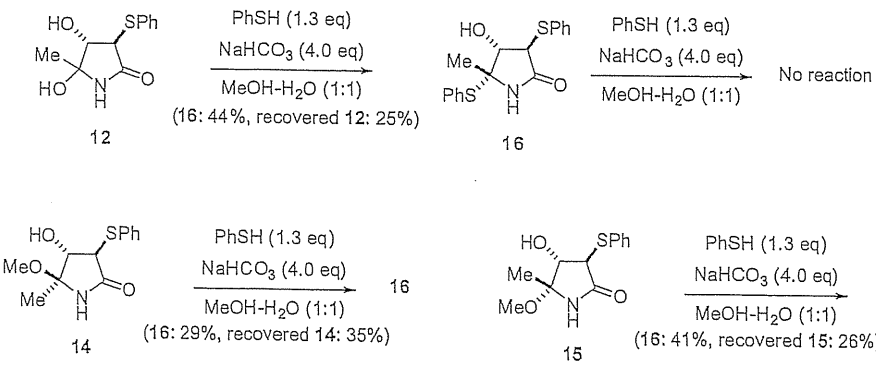

Scheme 8. Reaction of **12**, **14**, **15** or **16** with thiophenol.

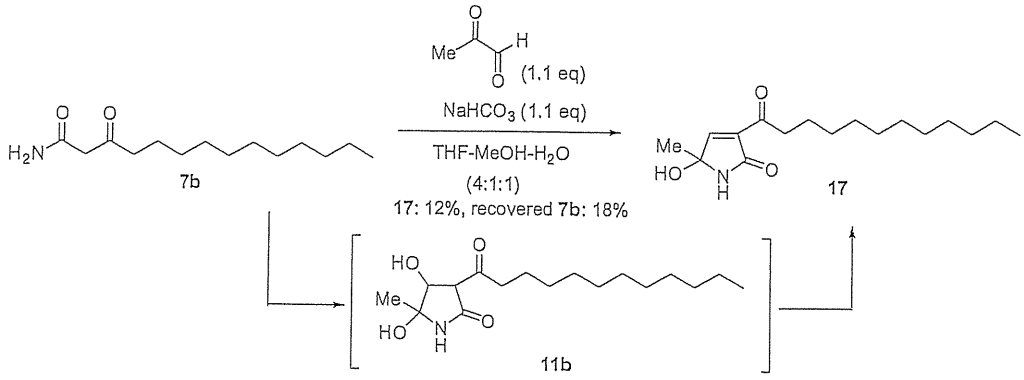

Scheme 9. Reaction of 7b with methyl glyoxal.

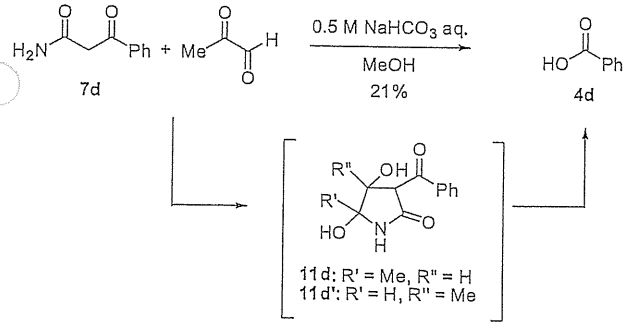

Scheme 10. Reaction of 7d with methyl glyoxal.

must involve a nucleophilic attack of the thiolate anion on the epoxide in **1a**. Water might be involved in the series of reactions. One possibility is that the hydrogen bond between the epoxide oxygen and water might activate the reactivity of the epoxide in **1a**.[31] It has been reported that cerulenin, a related natural product containing an α,β-epoxy-γ-lactam, reacts with thiol to form the cerulenin-thiol adduct in protic solvents (Scheme 11).[35,36] Cerulenin did not convert thiol into the corresponding disulfide, indicating that the acyl side-chain in epolactaene and its derivatives (**1**) is essential for disulfide formation.

The reactivity of **1** strongly depends on the acyl side-chain (Table 3). Reaction of **2** with **1a** and **1d**, which contain the unsaturated acyl side-chain gave disulfide **3** and carboxylic acid **4** (entries 1 and 5). Meanwhile, reaction of **2** with **1b**, which has a *n*-dodecanoyl side-chain, only gave the adduct **5b** (entry 2). Furthermore, reaction of **2** with **1c**, which has a *n*-hexanoyl side-chain, gave disulfide **3** and hexanoic acid **4c** as well as the adduct **5c** (entry 4). The difference of the reactivity might be explained by the solubility of the side-chain of **1** in polar solvent. The low solubility derived from the hydrophobic side-chain in the polar solvent might cause the sequential reactions to stop and thereby lower the production of the final disulfide. In the reaction of **1b** and **2**, the use of excess **2** recovered the production of **3** (entry 3). Because the adduct **5** was obtained in the reaction of **2** with **1b** or **1c** (Table 3, entries 3 and 4), the thiolate anion selectively attack the C-3 position on the epoxide in **1**. The regioselective epoxide opening might be due to the steric hindrance between the attacking thiolate and the substituent (methyl or hydroxyl group) at the C-5 position in the lactam ring.

The reaction of **1b** with 1.2 mol equiv of **2** gave the adduct **5b** as a sole product (entry 2 in Table 3). However, the reaction of **1b** with 1.0 equiv of thiophenol afforded the adduct **6b**, diphenyl disulfide, carboxylic acid **4b**, β-ketoamide **7b** and γ-lactam **8-Ph** (entry 1 in Table 4). These results indicate that the products of the reaction of **1b** with an almost equimolar amount of thiol depend on the thiol used in the reaction. By contrast, similar products were obtained when the thiol was present in excess (entry 3 in Table 3 and entry 2 in Table 4). The products obtained by the reaction of **1b** with 2.0 equiv of **2** or thiophenol were the disulfide, **4b** and the adduct (**5b** or **6b**).

Previously, we proposed the mechanism of the reaction of **1b** with **2** as shown in Scheme 2.[24] However, the present studies reveal that the proposed mechanism is incorrect because a retro-Claisen reaction of **5b** and the reaction of **9** with **2** under basic conditions did not proceed (Schemes 3 and 4). Thus, we have reexamined the mechanism of the reaction of **1** and thiol.

We found that reaction of the α-sulfanyl-β-ketoamide **6b** with methyl glyoxal under basic conditions afforded carboxylic acid **4b** and γ-lactams **12**, **14** and **15** (Scheme 7). This result indicates that compound **10** is liable to cleavage by a retro-Claisen reaction (Scheme 6). The formation of **8-Ph** in the reaction between **1b** and thiophenol also supports this conclusion (Table 4, entry 1).

We also found that reaction of the β-ketoamide **7d** with methyl glyoxal under basic conditions afforded carboxylic acid **4d** (Scheme 10). The formation of **4d** should come from the initial formation of **11d** or **11d'**, followed by a retro-Claisen reaction. Although the formation of **4b** was not observed in the reaction of **7b** and methyl glyoxal (Scheme 9), the result obtained by the reaction of **7d** with methyl glyoxal suggests that the formation of carboxylic acid **4** in the reaction of **1** with thiol may be derived from the retro-Claisen reaction of **11** (Scheme 6).

As a result of these findings, we have revised the mechanism of the disulfide formation of thiol induced by **1** (Scheme 12). The reaction involves nucleophilic attack of the initial thiolate anion

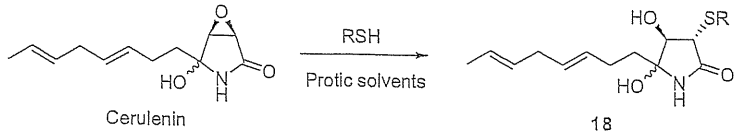

Scheme 11. Reported reaction between cerulenin and thiols to form the cerulenin-thiol adduct.

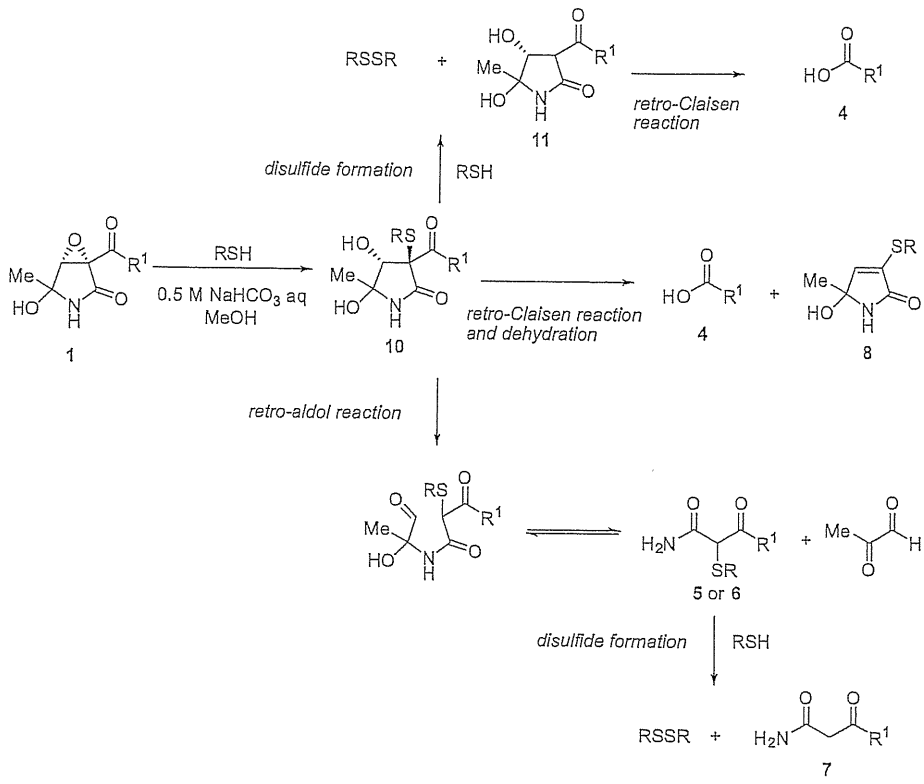

Scheme 12. Revision of our proposed mechanism according to the results obtained in this study.

on the epoxide in **1** to give the adduct **10**. Then the subsequent attack of the second thiolate anion on the sulfur atom in **10** may produce the disulfide, accompanied by the formation of **11**. Compound **11** may be cleaved by a retro-Claisen reaction to yield the carboxylic acid **4**. The formation of the adduct **5** or **6** is explained by a retro-aldol reaction of **10** followed by elimination of methyl glyoxal. The alternative disulfide may be caused by the reaction of **5** or **6** with the second thiolate anion. One of the side reactions is a retro-Claisen reaction of **10** to give **4** and the γ-lactam **8**.

4. Conclusion

In this paper, we investigated the thiolysis and disulfide formation of epolactaene and its derivatives. We examined the disulfide formation using various thiols and epolactaene derivatives as well as the mechanistic studies using thiolysis products. As a result of these studies, we have revised our proposed mechanism of disulfide formation induced by epolactaene and its derivatives. We believe that our present studies will be invaluable not only for analyzing the molecular and cellular biological activities of epolactaene and its derivatives, but also in the development of new reagents for disulfide bond formation.

5. Experimental procedure

5.1. General information

^{1}H and ^{13}C NMR spectra were recorded on a JEOL 270 MHz spectrometer (EX-270W) or a Bruker 600 MHz spectrometer (Avance DRX-600). Chemical shifts are expressed in δ (ppm) relative to Me_4Si or the residual solvent resonance, and coupling constants (J) are expressed in Hertz. Melting point (Mp) data were determined with a Yanaco MP-3S instrument and were uncorrected. Optical rotation data were recorded on a Jasco P-1030 digital polarimeter. Infrared (IR) spectra were recorded on a Jasco FT/IR-410 spectrometer, using NaCl (neat) or KBr pellet (solid). Mass spectra (MS) were obtained on an Applied Biosystems mass spectrometer (API QSTAR pulsar i) under high-resolution conditions or Varian 910-MS Fourier transform mass spectrometer. Analytical thin-layer chromatography was performed on Silica Gel 60 F254 plates (Merck, Germany). Flash chromatography was carried out on PSQ 100B (Fuji Silysia Co., Japan).

5.2. General method for the disulfide formation of *N*-acetyl-L-cysteine methyl ester (2) induced by epolactaene (1a) (Table 1)

A degassed solution of **1** (1.0 equiv) and **2** (2.0–2.3 mol equiv) in the solvent indicated in Table 1 was stirred at room temperature under a nitrogen atmosphere until no further change in TLC was observed. The reaction was quenched by the addition of 1 M HCl aqueous solution, and the mixture was diluted with EtOAc. The layers were separated, the aqueous layer was extracted with EtOAc. The combined organic layer was washed with brine, dried (Na_2SO_4) and concentrated. The residue was purified by column chromatography (hexane/EtOAc = 1:1, then $CHCl_3$/MeOH = 20:1) to give **3** and **4a**. The structures of **3** and **4a** were confirmed by comparison of the ^{1}H NMR data with those reported.

5.3. General procedure for the formation of disulfides (Table 2)

To a solution of **1** (10 mg, 26 μmol) and thiol (2.2 mol equiv) in degassed MeOH (1.0 mL) was added 0.5 M aqueous solution of $NaHCO_3$ (1.0 mL) at room temperature. The mixture was stirred at room temperature under a nitrogen atmosphere until no further

change in TLC was observed. The reaction was quenched by the addition of 1 M HCl aqueous solution, and the mixture was diluted with EtOAc. The layers were separated, the aqueous layer was extracted with EtOAc. The combined organic layer was washed with brine, dried (Na_2SO_4) and concentrated. The residue was purified by column chromatography to give the corresponding disulfide. The structures of diphenyl disulfide, 2,2′-dipyridyl disulfide, *n*-dihexyl disulfide and *n*-didodecyl disulfide were confirmed by MS analyses as well as comparison of the ^{1}H NMR data with those of the authentic disulfides.

5.4. (*1R,5R*)-1-Benzoyl-4-hydroxy-4-methyl-6-oxa-3-azabicyclo-[3.1.0]hexan-2-one (1d)

The titled compound was prepared according to the bridgehead oxiranyl anion strategy previously reported.[24] Compound **1d** was obtained as white solid. Mp = 137–139 °C. $[\alpha]_D^{23} = -54.7$ (*c* 0.20, MeOH). IR (KBr): 3286, 3062, 2990, 2922, 2853, 1691, 1651, 1540, 1486, 1447, 1409, 1354, 1266, 1177, 1110, 1050, 937, 879, 851, 787. 690 cm^{-1}. NMR data: compound **1d** was observed as a 5:1 diastereomeric mixture in CD_3OD. Peaks derived from the major isomer were indicated. ^{1}H NMR (600 MHz, CD_3OD): δ = 8.06 (2H, d, J = 7.9 Hz), 7.67 (1H, t, J = 7.9 Hz), 7.53 (2H, d, J = 7.9 Hz), 4.17 (1H, s), 1.56 (3H, s). ^{13}C NMR (125 MHz, CD_3OD): δ = 191.2, 171.8, 136.3, 135.5, 130.2 (×2), 129.9 (×2), 84.8, 66.2, 64.4, 22.2. HRMS (ESI): calcd for $C_{12}H_{11}NO_4Na$ ([M+Na]$^+$) 256.0580, found 256.0568.

5.5. General procedure for the reaction of 1 with 2 (Table 3)

To a solution of **1** (1.0 equiv) and **2** (1.2–2.0 mol equiv) in degassed MeOH (1.0 mL) was added 0.5 M aqueous solution of $NaHCO_3$ (1.0 mL) at room temperature. The mixture was stirred at room temperature under a nitrogen atmosphere until no further change in TLC was observed. The reaction was quenched by the addition of 1 M HCl aqueous solution, and the mixture was diluted with EtOAc. The layers were separated, the aqueous layer was extracted with EtOAc. The combined organic layer was washed with brine, dried (Na_2SO_4) and concentrated. The products were purified by column chromatography. The structures of **3**, **4a** and **5b** were confirmed by comparison of the ^{1}H NMR data with those reported. The structures of **4b**, **4c** and **4d** by MS analyses as well as comparison of the ^{1}H NMR data with those of the authentic carboxylic acids.

5.5.1. *N*-Acetyl-*S*-[1-(aminocarbonyl)-2-oxooctanyl]-L-cysteinate (5c)

Colorless oil. $[\alpha]_D^{23} = -12.3$ (*c* 0.21, MeOH). IR (neat): 3444, 3325, 3018, 2929, 2861, 1739, 1670, 1585, 1438, 1304, 1039, 667 cm^{-1}. ^{1}H NMR (270 MHz, $CDCl_3$ with 0.03% TFA): δ = 6.58 (1H, br s), 5.92 (1H, br s), 4.82 (1H, m), 3.82 (3H, s), 3.13 (1H, m), 2.98 (1H, m), 2.17 (3H, s), 1.63 (2H, m), 1.36–1.25 (8H, br m), 0.88 (3H, t, J = 6.9 Hz). ^{13}C NMR (100 MHz, $CDCl_3$ with 0.03% TFA): δ = 187.4, 175.6, 171.4, 170.7, 53.2, 52.8, 38.8, 34.2, 31.5, 29.7, 26.4, 22.8, 22.3, 13.8. HRMS (ESI): calcd for $C_{14}H_{24}N_2O_5NaS$ ([M+Na]$^+$) 355.1298, found 355.1298.

5.6. The reaction of 1b with thiophenol (Table 4)

To a solution of **1b** (34.5 mg, 0.11 mmol for entry 1) or (16.3 mg, 52.3 μmol for entry 2) and thiophenol (11 μL, 0.11 mmol) in degassed MeOH (2.0 mL) was added 0.5 M aqueous solution of $NaHCO_3$ (1.0 mL) at room temperature. The mixture was stirred at room temperature under a nitrogen atmosphere until no further change in TLC was observed. The reaction was quenched by the addition of 1 M HCl aqueous solution, and the mixture was diluted with EtOAc. The layers were separated, the aqueous layer was extracted with EtOAc. The combined organic layer was washed with brine, dried (Na_2SO_4) and concentrated. The products were purified by PTLC (hexane/EtOAc = 4:1). In entry 1, diphenyl disulfide (6.6 mg, 56%), **4b** (10.9 mg, 49%), **6b** (7.0 mg, 18%), **7b** (0.8 mg, 3%) and **8-Ph** (3.2 mg, 13%) were obtained. In entry 2, diphenyl disulfide (10.0 mg, 85%), **4b** (2.1 mg, 20%) and **6b** (1.7 mg, 9%) were obtained. The structures of diphenyl disulfide and dodecanoic acid **4b** were confirmed by MS analyses as well as comparison of the ^{1}H NMR data with those of the authentic samples.

5.6.1. 3-Oxo-2-phenylsulfanyltetradecanamide (6b)

Yellow oil. IR (neat): 3452, 3309, 3234, 3176, 2925, 2856, 1722, 1637, 1585, 1468, 1412, 1329, 957 cm^{-1}. ^{1}H NMR (270 MHz, $CDCl_3$): δ = 7.29 (2H, d, J = 7.6 Hz), 7.14 (2H, d, J = 7.6 Hz), 7.14 (1H, t, J = 7.6 Hz), 6.72 (1H, br s), 5.27 (1H, br s), 2.62 (2H, t, J = 7.6 Hz), 1.58 (2H, m), 1.21 (16H, br m), 0.88 (3H, t, J = 6.8 Hz), −4.14 (1H, s). ^{13}C NMR (68 MHz, $CDCl_3$): δ = 188.5, 174.8, 137.0, 129.0 (×2), 125.4, 124.8 (×2), 89.4, 34.1, 32.0, 29.7 (×2), 29.5, 29.4, 29.3, 29.3, 26.7, 22.8, 14.2. HRMS (ESI): calcd for $C_{20}H_{31}NO_2NaS$ ([M+Na]$^+$) 372.1973, found 372.1968.

5.6.2. 3-Oxotetradecanamide (7b)

White solid. Mp = 117 °C. IR (KBr): 3377, 3186, 2920, 2852, 1707, 1651, 1635, 1431, 1130, 721 cm^{-1}. ^{1}H NMR (270 MHz, $CDCl_3$): δ = 7.07 (1H, br s), 5.59 (1H, br s), 3.43 (2H, s), 2.53 (2H, t, J = 7.3 Hz), 1.59 (2H, m), 1.26 (16H, br s), 0.88 (3H, t, J = 7.0 Hz). ^{13}C NMR (68 MHz, $CDCl_3/CD_3OD$ = 4:1): δ = 205.9, 169.2, 43.3, 31.7, 29.4 (×3), 29.2, 29.1, 29.1, 28.8, 23.1, 22.4, 14.8. HRMS (ESI): calcd for $C_{14}H_{27}NO_2Na$ ([M+Na]$^+$) 264.1934, found 264.1940.

5.6.3. 5-Hydroxy-5-methyl-3-phenylsulfanyl-3-pyrrolin-2-one (8-Ph)

Amorphous solid. IR (film): 3384, 3219, 3018, 2978, 2929, 1700, 1577, 1477, 1440, 1419, 1377, 1356, 1151, 1097, 1026, 1003, 943, 831 cm^{-1}. ^{1}H NMR (270 MHz, $CDCl_3$): δ = 7.56 (2H, m), 7.42 (3H, m), 6.68 (1H, br s), 6.00 (1H, s), 2.96 (1H, br s), 1.55 (3H, s). ^{13}C NMR (125 MHz, $CDCl_3$): δ = 168.3, 138.8, 137.9, 134.3 (×2), 129.8 (×2), 129.41, 129.37, 86.5, 24.9. HRMS (ESI): calcd for $C_{11}H_{11}NO_2NaS$ ([M+Na]$^+$) 244.0403, found 244.0401.

5.7. Treatment of 5b in a 1:1 MeOH/0.5 M $NaHCO_3$ aqueous solution (Scheme 3A)

To a solution of **5b** (10.3 mg, 24.7 μmol) in degassed MeOH (1.0 mL) was added 0.5 M aqueous solution of $NaHCO_3$ (1.0 mL) at room temperature. The mixture was stirred at room temperature under a nitrogen atmosphere for 24 h. The reaction was quenched by the addition of 1 M HCl aqueous solution, and the mixture was diluted with EtOAc. The layers were separated, the aqueous layer was extracted with EtOAc. The combined organic layer was washed with brine, dried (Na_2SO_4) and concentrated. The residue was purified by column chromatography (hexane/EtOAc = 3:1, then $CHCl_3$/MeOH = 20:1) to give the recovered **5b** (5.8 mg, 58%). The specific rotation of **5b** decreased from $[\alpha]_D^{21} = -12.8$ (*c* 0.50, MeOH) to $[\alpha]_D^{21} = -0.9$ (*c* 0.29, MeOH) after treatment of **5b** under the basic conditions for 24 h

5.8. Treatment of 5b with 2 in a 1:1 MeOH/0.5 M $NaHCO_3$ aqueous solution (Scheme 3B)

To a solution of **5b** (5.8 mg, 13.9 μmol) and **2** (3.0 mg, 16.9 μmol) in degassed MeOH (1.0 mL) was added 0.5 M aqueous solution of $NaHCO_3$ (1.0 mL) at room temperature. The mixture was stirred at room temperature under a nitrogen atmosphere for 16 h. The reaction was quenched by the addition of 1 M HCl

aqueous solution, and the mixture was diluted with EtOAc. The layers were separated, the aqueous layer was extracted with EtOAc. The combined organic layer was washed with brine, dried (Na_2SO_4) and concentrated. The residue was purified by column chromatography ($CHCl_3$/MeOH = 20:1) to give **3** (1.7 mg, 35%), **7b** (0.6 mg, 17%) and the recovered **5b** (2.8 mg, 48%).

5.9. Methyl *N*-acetyl-*S*-(2-amino-2-oxoethyl)-L-cysteinate (9)

To a solution of **2** (26.7 mg, 0.15 mmol) in THF (2 mL) was added NaH (7.0 mg, 60% dispersion in mineral oil, 0.18 mmol) at 0 °C and the mixture was stirred at 0 °C for 10 min. To the solution was added 2-iodoacetamide (28.8 mg, 0.16 mmol) was added at 0 °C, and the mixture was stirred at room temperature for 3 h. The reaction was quenched by the addition of 1 M HCl aqueous solution, and the mixture was diluted with EtOAc. The layers were separated, the aqueous layer was saturated with NaCl and extracted with $CHCl_3$ (×13 times). The combined organic layer was dried (Na_2SO_4) and concentrated. The residue was purified by column chromatography ($CHCl_3$/MeOH = 20:1–10:1) to give **9** (7.8 mg, 22%) as white solid. Mp = 154–155 °C. $[\alpha]_D^{23} = -39.6$ (*c* 0.47, MeOH). IR (KBr): 3359, 3178, 3022, 2927, 1738, 1637, 1533, 1425, 1387, 1128, 1088 cm^{-1}. ^1H NMR (270 MHz, CD_3OD): δ = 4.66 (1H, dd, *J* = 8.4 Hz, 5.1 Hz), 3.73 (3H, s), 3.24 (1H, d, *J* = 14.9 Hz), 3.21 (1H, d, *J* = 14.9 Hz), 3.09 (1H, dd, *J* = 14.0 Hz, 5.1 Hz), 2.93 (1H, dd, *J* = 14.0 Hz, 8.4 Hz), 1.99 (3H, s). ^{13}C NMR (68 MHz, CD_3OD): δ = 174.6, 173.1, 172.3, 53.5, 52.9, 36.0, 34.9, 22.4. HRMS (ESI): calcd for $C_8H_{14}N_2O_4NaS$ ($[M+Na]^+$) 257.0566, found 257.0559.

5.9.1. Reaction of 9 with 2 in a 1:1 MeOH/0.5 M $NaHCO_3$ aqueous solution (Scheme 4)

To a solution of **9** (7.8 mg, 33.3 μmol) and **2** (7.1 mg, 40.1 μmol) in degassed MeOH (1.0 mL) was added 0.5 M aqueous solution of $NaHCO_3$ (1.0 mL) at room temperature. The mixture was stirred at room temperature under a nitrogen atmosphere for 25 h. The reaction was quenched by the addition of 1 M HCl aqueous solution, and the mixture was diluted with EtOAc. The layers were separated, the aqueous layer was extracted with EtOAc. The combined organic layer was washed with brine, dried (Na_2SO_4) and concentrated. The residue was purified by column chromatography ($CHCl_3$/MeOH = 20:1) to give the recovered **2** (4.9 mg, 69%).

5.10. Reaction of 6b with thiophenol in a 1:1 MeOH/0.5 M $NaHCO_3$ aqueous solution (Scheme 5)

To solution of **6b** (17.9 mg, 51.2 μmol) and thiophenol (7.0 μL, 68.4 μmol) in degassed MeOH (0.5 mL) was added 0.5 M aqueous solution of $NaHCO_3$ (0.5 mL) at room temperature. The mixture was stirred at room temperature under a nitrogen atmosphere for 21 h. The reaction was quenched by the addition of 1 M HCl aqueous solution, and the mixture was diluted with EtOAc. The layers were separated, the aqueous layer was extracted with EtOAc. The combined organic layer was washed with brine, dried (Na_2SO_4) and concentrated. The residue was purified by column chromatography (hexane/EtOAc = 20:1–10:1–4:1–1:1) to give diphenyl disulfide (8.3 mg, 74%) and **7b** (8.8 mg, 71%).

5.11. Reaction of 6b with methyl glyoxal in a 1:1 MeOH/0.5 M $NaHCO_3$ aqueous solution (Scheme 7A)

To solution of **6b** (5.9 mg, 16.9 μmol) and methyl glyoxal (12.0 μL, 40% solution in water, 66.6 μmol) in MeOH (0.5 mL) was added 0.5 M aqueous solution of $NaHCO_3$ (0.5 mL) at room temperature. The mixture was stirred at room temperature under a nitrogen atmosphere for 1 hour. The reaction was quenched by the addition of 1 M HCl aqueous solution, and the mixture was diluted with EtOAc. The layers were separated, the aqueous layer was extracted with EtOAc. The combined organic layer was washed with brine, dried (Na_2SO_4) and concentrated. The residue was purified by column chromatography (hexane/EtOAc = 2:1) to give **4b** (3.4 mg, quant).

5.12. Reaction of 6b with methyl glyoxal in the presence of $NaHCO_3$ in a 4:1:1 THF/MeOH/H_2O solution (Scheme 7B)

To solution of **6b** (74.2 mg, 0.21 mmol) and methyl glyoxal (150 μL, 40% solution in water, 0.83 mmol) in THF/MeOH/H_2O (4:1:1, 6 mL) was added $NaHCO_3$ (56.3 mg, 0.67 mmol) at room temperature. The mixture was stirred at room temperature under a nitrogen atmosphere for 24 hours. The reaction was quenched by the addition of 1 M HCl aqueous solution, and the mixture was diluted with EtOAc. The layers were separated, the aqueous layer was extracted with EtOAc. The combined organic layer was washed with brine, dried (Na_2SO_4) and concentrated. The residue was purified by column chromatography (EtOAc/MeOH = 20:1) and preparative TLC (hexane/EtOAc = 1:3) to give **4b** (36.6 mg, 86%), **12** (18.2 mg, 36%), **13** (7.8 mg, 17%), **14** (2.5 mg, 5%) and **15** (2.3 mg, 4%).

5.12.1. (3*R**,4*S**,5*RS*)-4,5-Dihydroxy-5-methyl-3-phenylsulfanyl-2-pyrrolidinone (12)

Colorless oil. IR (film): 3282, 3008, 2929, 2862, 1705, 1583, 1471, 1429, 1383, 1128, 1053, 997 cm^{-1}. Compound **12** was observed as a 4:1 diastereomeric mixture in DMSO-d_6. The data for major diastereomer was indicated. ^1H NMR (270 MHz, DMSO-d_6): δ = 8.59 (1H, s), 7.46 (2H, m), 7.31 (2H, m), 7.24 (1H, m), 5.58 (1H, d, *J* = 7.0 Hz), 5.46 (1H, s), 3.82 (1H, d, *J* = 8.9 Hz), 3.63 (1H, dd, *J* = 8.9 Hz, 7.0 Hz), 1.27 (3H, s). ^{13}C NMR (68 MHz, DMSO-d6): δ = 170.9, 135.0, 130.3 (×2), 128.9 (×2), 126.6, 83.9, 77.3, 53.3, 25.2. HRMS (ESI): calcd for $C_{11}H_{13}NO_3NaS$ ($[M+Na]^+$) 262.0508, found 262.0510.

5.12.2. 5-Hydroxy-4-methyl-3-phenylsulfanyl-3-pyrrolin-2-one (13)

White solid. Mp = decomposition with browning at 130 °C. IR (film): 3298, 3066, 3016, 2925, 2858, 1697, 1579, 1469, 1339, 1218, 1184, 1084, 1034, 883 cm^{-1}. ^1H NMR (270 MHz, $CDCl_3$): δ = 7.33 (1H, s), 7.30–7.17 (5H, m), 5.34 (1H, br s), 4.23 (1H, br s), 2.06 (3H, s). ^{13}C NMR (68 MHz, $CDCl_3$): δ = 170.6, 133.4, 133.1, 129.1 (×2), 129.0 (×3), 126.6, 81.2, 13.3. HRMS (ESI): calcd for $C_{11}H_{11}NO_2NaS$ ($[M+Na]^+$) 244.0403, found 244.04010.

5.12.3. (3*R**,4*S**,5*S**)-4-Hydroxy-5-methoxy-5-methyl-3-phenylsulfanyl-2-pyrrolidinone (14)

Amorphous solid. IR (film): 3398, 3276, 3008, 2935, 1705, 1585, 1468, 1427, 1389, 1352, 1302, 1176, 1107, 918, 876, 833 cm^{-1}. ^1H NMR (270 MHz, $CDCl_3$): δ = 7.63–7.59 (2H, m), 7.34–7.29 (3H, m), 6.36 (1H, br s), 4.24 (1H, dd, *J* = 6.2 Hz, 4.9 Hz), 3.60 (1H, d, *J* = 6.2 Hz), 3.06 (3H, s), 2.50 (1H, d, *J* = 4.9 Hz), 1.45 (3H, s). ^{13}C NMR (68 MHz, $CDCl_3$): δ = 171.4, 133.0 (2C), 131.5, 129.1 (2C), 128.1, 91.3, 76.5, 55.1, 49.4, 20.2. HRMS (ESI): calcd for $C_{12}H_{15}NO_3NaS$ ($[M+Na]^+$) 276.0665, found 276.0668.

5.12.4. (3*R**,4*S**,5*R**)-4-Hydroxy-5-methoxy-5-methyl-3-phenylsulfanyl-2-pyrrolidinone (15)

Amorphous solid. IR (film): 3410, 3248, 3012, 2931, 1711, 1583, 1468, 1429, 1394, 1346, 1174, 1112, 1058, 920 cm^{-1}. ^1H NMR (270 MHz, $CDCl_3$): δ = 7.62–7.57 (2H, m), 7.32–7.27 (3H, m), 7.08 (1H, br s), 3.88 (1H, dd, *J* = 10.0 Hz, 8.6 Hz), 3.73 (1H, d, *J* = 8.6 Hz), 3.31 (3H, s), 2.84 (1H, d, *J* = 10.0 Hz), 1.45 (3H, s). ^{13}C NMR (68 MHz, $CDCl_3$): δ = 172.7, 133.3 (2C), 132.9, 128.9 (2C),

128.0, 86.8, 79.2, 55.1, 49.6, 19.8. HRMS (ESI): calcd for $C_{12}H_{15}NO_3$-NaS ([M+Na]$^+$) 276.0665, found 276.0665.

5.12.5. (3*R**,4*R**,5*R**)-4-Hydroxy-5-methyl-3,5-bis(phenylsulfanyl)-2-pyrrolidinone (16)

To a solution of **12** (13.0 mg, 54.3 μmol) and thiophenol (7.0 μL, 68.4 μmol) in MeOH/H_2O (1:1, 4 mL) was added $NaHCO_3$ (18.3 mg, 0.22 mmol) at room temperature, and the mixture was stirred at room temperature for 24 h. The reaction was quenched by the addition of 1 M HCl aqueous solution, and the mixture was diluted with EtOAc. The layers were separated, the aqueous layer was extracted with EtOAc. The combined organic layer was washed with brine, dried (Na_2SO_4) and concentrated. The residue was purified by preparative TLC (hexane/EtOAc = 1:3) to give **16** (8.0 mg, 44%) as amorphous solid and recovered **12** (3.3 mg, 25%). According to the same procedure, compound **16** was obtained from **14** or **15**. **16**: IR (film): 3406, 3068, 3016, 2927, 1709, 1581, 1475, 1437, 1387, 1336, 1176, 1078, 1037, 924 cm^{-1}. ^{1}H NMR (270 MHz, DMSO-d_6): δ = 8.73 (1H, s), 7.58–7.16 (10H, m), 6.42 (1H, d, J = 5.7 Hz), 3.90 (1H, dd, J = 10.0 Hz, 5.7 Hz), 3.36 (1H, d, J = 10.0 Hz), 1.46 (3H, s). ^{13}C NMR (68 MHz, $CDCl_3$): δ = 169.9, 137.7 (×2), 134.7, 130.7, 130.1 (×2), 129.1, 128.90 (×2), 128.87 (×2), 126.7, 79.6, 74.6, 54.0, 26.7. HRMS (ESI): calcd for $C_{17}H_{17}NO_2$-NaS_2 ([M+Na]$^+$) 354.0593, found 354.0592.

5.13. 3-Dodecanoyl-5-hydroxy-5-methyl-3-pyrrolin-2-one (17)

To solution of **7b** (50.0 mg, 0.21 mmol) and methyl glyoxal (41 mg, 40% solution in water, 0.23 mmol) in THF/MeOH/H_2O (4:1:1, 4.5 mL) was added $NaHCO_3$ (19.7 mg, 0.23 mmol) at room temperature. The mixture was stirred at room temperature under a nitrogen atmosphere for 24.5 h. The reaction was quenched by the addition of 1 M HCl aqueous solution, and the mixture was diluted with EtOAc. The layers were separated, the aqueous layer was extracted with EtOAc. The combined organic layer was washed with brine, dried (Na_2SO_4) and concentrated. The residue was purified by preparative TLC (hexane/EtOAc = 1:3) to give **17** (7.4 mg, 12%) as colorless oil and recovered **7b** (8.9 mg, 18%). **17**: IR (film): 3298, 2954, 2925, 2854, 1711, 1618, 1466, 1412, 1379, 1136, 1119, 943, 667 cm^{-1}. ^{1}H NMR (270 MHz, DMSO-d_6): δ = 8.66, (1H, br s), 7.52 (1H, d, J = 1.6 Hz), 6.01 (1H, s), 2.80 (2H, t, J = 7.0 Hz), 1.48 (2H, m), 1.41 (3H, s), 1.24 (16H, m), 0.86 (3H, t, J = 6.2 Hz). ^{13}C NMR (68 MHz, DMSO-d_6): δ = 197.0, 167.1, 156.5, 134.0, 83.8, 32, 31.5, 29.2 (2C), 29.1, 29.0, 28.9, 28.7, 25.0, 23.2, 22.3, 14.2. HRMS (ESI): calcd for $C_{17}H_{29}NO_3Na$ ([M+Na]$^+$) 318.2040, found 318.2039.

5.14. Reaction of 7d with methyl glyoxal in a 1:1 MeOH/0.5 M $NaHCO_3$ aqueous solution (Scheme 10)

To solution of **7d** (22.6 mg, 0.14 mmol) and methyl glyoxal (29.7 mg, 40% solution in water, 0.16 mmol) in MeOH (1.0 mL) was added 0.5 M aqueous solution of $NaHCO_3$ (1.0 mL) at room temperature. The mixture was stirred at room temperature under a nitrogen atmosphere for 22.5 h. The reaction was quenched by the addition of 1 M HCl aqueous solution, and the mixture was diluted with EtOAc. The layers were separated, the aqueous layer was extracted with EtOAc. The combined organic layer was washed with brine, dried (Na_2SO_4) and concentrated. The residue was purified by preparative TLC (hexane/EtOAc = 1:3) to give **4d** (3.6 mg, 21%).

References and notes

1. Lees, W. J. *Curr. Opin. Chem. Biol.* 2008, *12*, 740.
2. Sevier, C. S.; Kaiser, C. A. *Antioxid. Redox Signal.* 2006, *8*, 797.
3. Bulaj, G. *Biotechnol. Adv.* 2005, *23*, 87.
4. Ishikawa, H.; Kim, S.; Kwak, K.; Wakasugi, K.; Fayer, M. D. *Proc. Natl. Acad. Sci. U.S.A.* 2007, *104*, 19309.
5. Piotukh, K.; Kosslick, D.; Zimmermann, J.; Krause, E.; Freund, C. *Free Radical Biol. Med.* 2007, *43*, 1263.
6. Lee, C.; Lee, S. M.; Mukhopadhyay, P.; Kim, S. J.; Lee, S. C.; Ahn, W. S.; Yu, M. H.; Storz, G.; Ryu, S. E. *Nat. Struct. Mol. Biol.* 2004, *11*, 1179.
7. Riemer, J.; Bulleid, N.; Herrmann, J. M. *Science* 2009, *324*, 1284.
8. Rietsch, A.; Beckwith, J. *Annu. Rev. Genet.* 1998, *32*, 163.
9. Messens, J.; Collet, J. F. *Int. J. Biochem. Cell Biol.* 2006, *38*, 1050.
10. Cumming, R. C.; Andon, N. L.; Haynes, P. A.; Park, M.; Fischer, W. H.; Schubert, D. *J. Biol. Chem.* 2004, *279*, 21749.
11. Kakeya, H.; Takahashi, I.; Okada, G.; Isono, K.; Osada, H. *J. Antibiot.* 1995, *48*, 733.
12. Kakeya, H.; Onozawa, C.; Sato, M.; Arai, K.; Osada, H. *J. Med. Chem.* 1997, *40*, 391.
13. Nagumo, Y.; Kakeya, H.; Shoji, M.; Hayashi, Y.; Dohmae, M.; Osada, H. *Biochem. J.* 2005, *387*, 835.
14. Nagumo, Y.; Kakeya, H.; Yamaguchi, J.; Uno, T.; Shoji, M.; Hayashi, Y.; Osada, H. *Bioorg. Med. Chem. Lett.* 2004, *14*, 4425.
15. Nakai, J.; Kawada, K.; Nagata, S.; Kuramochi, K.; Uchiro, H.; Kobayashi, S.; Ikekita, M. *Biochim. Biophys. Acta* 2002, *1581*, 1.
16. Kuramochi, K.; Matsui, R.; Matsubara, Y.; Nakai, J.; Sunoki, T.; Arai, S.; Nagata, S.; Nagahara, Y.; Mizushina, Y.; Ikekita, M.; Kobayashi, S. *Bioorg. Med. Chem.* 2006, *14*, 2151.
17. Mizushina, Y.; Kobayashi, S.; Kuramochi, K.; Nagata, S.; Sugawara, F.; Sakaguchi, K. *Biochem. Biophys. Res. Commun.* 2000, *273*, 784.
18. Kuramochi, K.; Mizushina, Y.; Nagata, S.; Sugawara, F.; Sakaguchi, K.; Kobayashi, S. *Bioorg. Med. Chem.* 2004, *12*, 1983.
19. Mizushina, Y.; Kuramochi, K.; Ikawa, H.; Kuriyama, I.; Shimazaki, N.; Takemura, M.; Oshige, M.; Yoshida, H.; Koiwai, O.; Sugawara, F.; Kobayashi, S.; Sakaguchi, K. *Int. J. Mol. Med.* 2005, *15*, 785.
20. Kuramochi, K.; Itaya, H.; Nagata, S.; Takao, K.; Kobayashi, S. *Tetrahedron Lett.* 1999, *40*, 7367.
21. Kuramochi, K.; Nagata, S.; Itaya, H.; Takao, K.; Kobayashi, S. *Tetrahedron Lett.* 1999, *40*, 7371.
22. Kuramochi, K.; Nagata, S.; Itaya, H.; Matsubara, Y.; Sunoki, T.; Uchiro, H.; Takao, K.; Kobayashi, S. *Tetrahedron* 2003, *59*, 9743.
23. Total synthesis of epolactaene: (a) Hayashi, Y.; Narasaka, K. *Chem. Lett.* 1998, 313; (b) Hayashi, Y.; Kanayama, J.; Yamaguchi, J.; Shoji, M. *J. Org. Chem.* 2002, *67*, 9443; (c) Marumoto, S.; Kogen, H.; Naruto, S. *J. Org. Chem.* 1998, *63*, 2068; (d) Marumoto, S.; Kogen, H.; Naruto, S. *Tetrahedron* 1999, *55*, 7129; (e) Marumoto, S.; Kogen, H.; Naruto, S. *Tetrahedron* 1999, *55*, 7145; (f) Tan, Z.; Negishi, E. *Org. Lett.* 2006, *8*, 2783.
24. Kuramochi, K.; Yukizawa, S.; Ikeda, S.; Sunoki, T.; Arai, S.; Matsui, R.; Morita, A.; Mizushina, Y.; Sakaguchi, K.; Sugawara, F.; Ikekita, M.; Kobayashi, S. *Bioorg. Med. Chem.* 2008, *16*, 5039.
25. Sayer, J. M.; Conlon, P.; Hupp, J.; Fancher, J.; Belanger, R.; White, E. J. *J. Am. Chem. Soc.* 1979, *101*, 1890.
26. Loechler, E. L.; Hollocher, T. C. *J. Am. Chem. Soc.* 1980, *102*, 7312.
27. Forsyth, D. A.; Hanley, J. A. *J. Am. Chem. Soc.* 1987, *109*, 7930.
28. Sato, S.; Sakai, R.; Kodama, M. *Bioorg. Med. Chem. Lett.* 2000, *10*, 1787.
29. Sakamoto, S.; Sato, S.; Ogata, T.; Kodama, M. *Fish. Sci.* 2000, *66*, 136.
30. Wu, J.; Xia, H. G. *Green Chem.* 2005, *7*, 708.
31. Mukherjee, C.; Maiti, G. H.; Misra, A. K. *ARKIVOC* 2008, 46.
32. Magnus, P.; Katoh, T.; Matthew, I. R.; Huffman, J. C. *J. Am. Chem. Soc.* 1989, *111*, 6707.
33. Durman, J.; Elliott, J.; McElroy, A. B.; Warren, S. *J. Chem. Soc., Perkin Trans. 1* 1985, 1237.
34. Girotra, N. N.; Wendler, N. L. *Tetrahedron Lett.* 1979, *20*, 4793.
35. Funabashi, H.; Iwasaki, S.; Okuda, S.; Ōmura, S. *Tetrahedron Lett.* 1983, *24*, 2673.
36. Funabashi, H.; Kawaguchi, A.; Tomoda, H.; Ōmura, S.; Okuda, S.; Iwasaki, S. *J. Biochem. (Tokyo)* 1989, *105*, 751.

Author's Choice

THE JOURNAL OF BIOLOGICAL CHEMISTRY VOL. 287, NO. 6, pp. 3885–3897, February 3, 2012

AMF-26, a Novel Inhibitor of the Golgi System, Targeting ADP-ribosylation Factor 1 (Arf1) with Potential for Cancer Therapy*[S]

Received for publication, October 25, 2011, and in revised form, December 6, 2011 Published, JBC Papers in Press, December 9, 2011, DOI 10.1074/jbc.M111.316125

Yoshimi Ohashi[‡], Hiroshi Iijima[§], Noriyuki Yamaotsu[§], Kanami Yamazaki[‡], Shigeo Sato[¶], Mutsumi Okamura[‡], Kenji Sugimoto[‖], Shingo Dan[‡], Shuichi Hirono[§], and Takao Yamori[‡1]

From the Division of [‡]Molecular Pharmacology and [¶]Experimental Chemotherapy, Cancer Chemotherapy Center, Japanese Foundation for Cancer Research, Tokyo 135-8550, Japan, the [§]School of Pharmacy, Kitasato University, Tokyo 108-8641, Japan, and the [‖]Laboratory of Applied Molecular Biology, Division of Applied Biochemistry, Graduate School of Agriculture and Biological Sciences, Osaka Prefecture University, Osaka 599-8531, Japan

Background: Golgi is a potential target for cancer treatment, but no inhibitor became an anticancer drug.
Results: Using a unique bioinformatics approach, we identified a novel Golgi inhibitor, AMF-26, targeting Arf1 activation and possessing potent antitumor activity.
Conclusion: AMF-26 is a promising new anticancer drug lead.
Significance: Our data indicate that Arf1 activation is a promising target for cancer treatment.

ADP-ribosylation factor 1 (Arf1) plays a major role in mediating vesicular transport. Brefeldin A (BFA), a known inhibitor of the Arf1-guanine nucleotide exchange factor (GEF) interaction, is highly cytotoxic. Therefore, interaction of Arf1 with ArfGEF is an attractive target for cancer treatment. However, BFA and its derivatives have not progressed beyond the pre-clinical stage of drug development because of their poor bioavailability. Here, we aimed to identify novel inhibitors of the Arf1-ArfGEF interaction that display potent antitumor activity *in vivo* but with a chemical structure distinct from that of BFA. We exploited a panel of 39 cell lines (termed JFCR39) coupled with a drug sensitivity data base and COMPARE algorithm, resulting in the identification of a possible novel Arf1-ArfGEF inhibitor AMF-26, which differed structurally from BFA. By using a pulldown assay with GGA3-conjugated beads, we demonstrated that AMF-26 inhibited Arf1 activation. Subsequently, AMF-26 induced Golgi disruption, apoptosis, and cell growth inhibition. Computer modeling/molecular dynamics (MD) simulation suggested that AMF-26 bound to the contact surface of the Arf1-Sec7 domain where BFA bound. AMF-26 affected membrane traffic, including the *cis*-Golgi and *trans*-Golgi networks, and the endosomal systems. Furthermore, using AMF-26 and its derivatives, we demonstrated that there was a significant correlation between cell growth inhibition and Golgi disruption. In addition, orally administrated AMF-26 (83 mg/kg of body weight; 5 days) induced complete regression of human breast cancer BSY-1 xenografts *in vivo*, suggesting that AMF-26 is a novel anticancer drug candidate that inhibits the Golgi system, targeting Arf1 activation.

Protein-protein interactions (PPIs)[2] play an important role in many biological processes, such as growth, cell survival, and intercellular signal transduction (1, 2). Therefore, inhibitors of specific PPIs can act as novel therapeutic agents including anticancer drugs. Indeed, several small molecule-PPI inhibitors have been developed, such as Nutlin-3 for HDM2-p53 interaction (3), and ABT-737, a Bcl-2 family protein inhibitor (4). Nonetheless, the number of promising PPI inhibitors for cancer treatment remains limited.

In this study, we focused on the activation of ADP-ribosylation factors (Arfs) by its guanine nucleotide exchange factors (GEFs). Arfs are members of the Ras superfamily of small GTPases that play a major role in mediating vesicular transport in the secretory and endocytic pathways (5). The cellular activity of Arfs is stimulated by the Sec7 domain of GEFs that promote the exchange of inactive GDP-bound forms to active GTP-bound forms (6). Arf1, the best characterized Arf, localizes primarily to the Golgi apparatus and regulates both anterograde and retrograde vesicular traffic (7). The first identified small molecule PPI that targets the interaction between Arf-ArfGEF was brefeldin A (BFA, Fig. 1*A*), a lactone isolated from fungi, which inhibits the activation of Arf1 by a subset of its GEFs (8, 9). Treatment of BFA causes rapid but reversible disruption of the Golgi apparatus leading to the vesiculation of the *cis*-Golgi and *trans*-Golgi network (TGN) (10, 11). Furthermore, BFA showed tumor growth inhibition *in vitro* (12) and *in vivo* at an early stage (13). Therefore, inhibitors of Arf1-ArfGEF interaction are valuable tools for studying membrane traffic as well as anticancer drug candidates. However, BFA and its deriv-

* This work was supported by Grants-in-aid for Scientific Research (A) 22240092 from the Japan Society for the Promotion of Science (to T. Y.) and Grant-in-aid for Scientific Research on Priority Areas 11177101 from the Ministry of Education, Culture, Sports, Science and Technology (to T. Y.).
Author's Choice—Final version full access.
[S] This article contains supplemental Tables S1 and S2, Fig. S1, "Experimental Procedures," and Video S1.
[1] To whom correspondence should be addressed. Tel.: 81-3-3520-0111; Fax: 81-3-3570-0484; E-mail: yamori@jfcr.or.jp.

[2] The abbreviations used are: PPI, protein-protein interaction; Arf, ADP-ribosylation factor; BFA, brefeldin A; BIG, brefeldin A-inhibited guanine nucleotide-exchange proteins; CLCa, clathrin light chain a; COP, coat protein complex; ER, endoplasmic reticulum; ERGIC, ER-Golgi intermediate compartment; GBF1, Golgi-specific brefeldin A resistance factor 1; GEF, guanine nucleotide exchange factor; JFCR39, a panel of 39 human cancer cell lines; TGN, *trans*-Golgi network; PARP, poly(ADP-ribose) polymerase; MD, molecular dynamics; HP, hydrophobic.

atives have not progressed beyond the pre-clinical stage of drug development (13, 14).

We previously established a panel of 39 cell lines (termed JFCR39) coupled with our own drug sensitivity data base, which is comparable with that of the NCI60 panel from the National Cancer Institute (NCI) (15–19). Using the COMPARE computer algorithm (details described under "Results"), it is possible to correlate the growth inhibitory patterns of JFCR39 (termed "fingerprints") of a test compound with those of known anticancer drugs and inhibitors (20, 21). Here, we have attempted to identify new Arf1-ArfGEF inhibitors with equivalent functions to BFA but with a different chemical structure, by using COMPARE-guided *in silico* screening instead of structure-based screening.

This approach enabled us to discover a novel small molecule AMF-26 (Fig. 1*B*), an octahydronaphthalene derivative, which disrupts the Golgi system probably by inhibiting the Arf1 activation. AMF-26 shows strong growth inhibition against JFCR39 cell lines *in vitro*. Furthermore, it showed potent antitumor activity against xenografts of the human breast cancer cell line BSY-1 via oral administration.

EXPERIMENTAL PROCEDURES

Chemicals—AMF-26 ((2*E*,4*E*)-5-((1*S*,2*S*,4a*R*,6*R*,7*S*,8*S*,8a*S*)-7-hydroxy-2,6,8-trimethyl-1,2,4a,5,6,7,8,8a-octahydronaphthalen-1-yl)-2-methyl-*N*-(pyridin-3-yl-methyl)penta-2,4-dienamide) and its derivatives were synthesized from AMF-14, a natural product from the genus *Trichoderma*, and kindly provided by the Research Laboratories Kyoto, Nippon Shinyaku Co., Ltd. (Kyoto, Japan). Details of the synthesis methods and the chemical properties of the final product are described under supplemental "Experimental Procedures." BFA and nocodazole were purchased from Sigma, and bafilomycin A1 was purchased from Tocris Bioscience (Bristol, UK). For *in vitro* studies, these compounds were reconstituted to 10 mM in DMSO (Sigma) and stored at −20 °C. For animal experiments, AMF-26 was suspended in 0.05% Cremophor EL (Sigma-Aldrich) in water as a solid dispersion. The antibodies for immunostaining were as follows: monoclonal to anti-GBF1 (clone), anti-adaptin γ (clone 88), and anti-adaptin δ (clone 18) were purchased from BD Biosciences (San Jose, CA), anti-ERGIC53 (clone G1/93) was from ALEXIS Biochemicals (Farmingdale, NY), anti-Arf (clone 1D9) and anti-Arf1 (clone EP442Y) were from Abcam (Cambridge, United Kingdom), and anti-α tubulin (clone B-5-1-2) was from Sigma. Rabbit polyclonal to anti-βCOP was from Abcam, and anti-cleaved poly(ADP-ribose) polymerase (PARP) was from Cell Signaling Technology (Boston, MA). Fluorescent probe LysoTracker was purchased from Invitrogen. For Western blotting, horseradish peroxidase-conjugated donkey anti-rabbit or sheep anti-mouse IgG (GE Healthcare) was used as a secondary antibody. For immunofluorescence microscopy, Alexa 488-conjugated goat anti-rabbit or anti-mouse IgG (Molecular Probes, Eugene, OR) was used as a secondary antibody.

Cell Lines—A panel of 39 human cancer cell lines (termed JFCR39, described previously (22)) was used for the *in vitro* experiments. BSY-1 (human breast cancer) cells were also used for *in vivo* studies. MDA-MB-435 (human breast cancer) cells stably expressing GFP-tagged human clathrin light chain a (MDA-MB-435/GFP-CLCa) were prepared as described previously (23). HEK293T (human embryonic kidney) cells were purchased from American Type Culture Collection (Manassas, VA). JFCR39 and MDA-MB-435/GFP-CLCa cells were cultured in RPMI 1640 medium (Wako Pure Chemical Industries) supplemented with 5% fetal bovine serum, penicillin (100 units/ml), and streptomycin (100 μg/ml) in a humidified atmosphere including 5% CO_2 at 37 °C. HEK293T was cultured in DMEM (Wako Pure Chemical Industries) supplemented with 10% heat-inactivated fetal bovine serum and kanamycin, at 37 °C under 5% CO_2. For *in vivo* studies, BSY-1 cells were grown as subcutaneous tumors in nude mice.

Analysis of Cell Growth Inhibition—The inhibition of cell proliferation was assessed by measuring changes in total cellular protein in a culture of each of the JFCR39 cell lines after 48 h of drug treatment by use of a sulforhodamine B assay (24). The 50% growth inhibition (GI_{50}) value was calculated as described previously (18, 19).

COMPARE Analysis—Based on these sets of GI_{50} values, fingerprints are presented in the graphic profiles of relative sensitivity within JFCR39. To analyze the correlation between the fingerprints of drug A and drug B, we exploited the COMPARE computer algorithm as described previously (18, 20, 22). The Pearson correlation coefficient between the fingerprints of drug A and drug B was calculated ($n = 39$).

Live Imaging—MDA-MB-435/GFP-CLCa cells were grown in a 35-mm glass-bottomed dish (Matsunami Glass Ind., Osaka, Japan) for 48 h. Subsequently, the cells were treated with chemicals and imaged on the temperature-controlled stage top incubator (Tokai Hit Co., Shizuoka, Japan) of fluorescent microscopy IX81 (Olympus Corp.) with a ×60 oil, NA 1.35 objective at 37 °C under 5% CO_2. Temperature and CO_2 concentration were maintained with an INUG2A control unit (Tokai Hit Co.). MetaMorph Software (Molecular Devices, Downingtown, PA) was used to control image acquisition and manipulation. For time-lapse observation, images were recorded as described previously by Sakaushi *et al.* (23).

Arf-GTP Pulldown Assay—The pulldown assay to estimate the signals of GTP-bound Arfs was performed as described previously (25, 26). Every pulldown assay was performed with the VHS and GAT domains of human GGA3, cloned, and purified according to a published protocol (25, 26) with modifications as described under supplemental "Experimental Procedures."

We examined the guanine nucleotide exchange activity of endogenous Arfs as follows. BSY-1 cells treated with chemicals for 1 h were scraped into 0.5 ml of cold pulldown buffer containing 50 mM Tris-HCl, pH 7.5, 100 mM NaCl, 2 mM $MgCl_2$, 0.1% SDS, 0.5% sodium deoxycholate, 1% Triton X-100, 10% glycerol, and protease inhibitors mixture (Nacalai Tesque Inc., Kyoto, Japan). The cell lysate was cleared using GSH-Sepharose 4B beads. Then the lysate was gently rotated with the beads containing 50 μg of rGST-GGA3 protein for 30 min at 4 °C. Bound proteins were washed three times with cold wash buffer (50 mM Tris-HCl, pH 7.5, 100 mM NaCl, 2 mM $MgCl_2$, 1% Nonidet P-40, 10% glycerol and protease inhibitors mixture), followed by boiling for 5 min with SDS sample buffer. Proteins in the samples were separated in 10–20% Multi-Gel II mini (Cosmo Bio Co., Tokyo, Japan), followed by electroblotting onto a polyvinylidene difluoride membrane (GE Healthcare).

After immunoblotting analysis using anti-*pan*-Arf and Arf1-specific antibody, immunoreactive bands were identified with the ECL Plus Western blotting detection system (GE Healthcare). Band intensity was determined using the program ImageJ (National Institute of Health).

To confirm the inhibitory efficacy of Arf1 activation, HEK293T/Arf1-HA cells were used to measure exogenous Arf1-GTP. Using the Lipofectamine 2000 reagent (Invitrogen) according to the manufacturer's instructions, HEK293T cells were transfected with the Arf1-HA expression vector, prepared as described under supplemental "Experimental Procedures." For transfection, HEK293T cells were seeded at a density of 3×10^6 cells/10 ml in a 10-cm plate. The transfectants were then incubated for 24 h, and subsequently treated with chemicals for 1 h. The cell lysates were assayed as described above. Because of a difference in molecular weight, the exogenous band of Arf1-HA can be differentiated from the endogenous band of intact Arf1. In HEK293T/Arf1-HA cells, the expression of intact Arf1 was very low. Therefore, the intensity of the band corresponding to Arf1 was apparently weaker than that of the exogenous Arf1-HA.

Conformational Sampling of AMF-26—Conformational analysis of AMF-26 was performed on an Apple Power Mac G5 (PowerPC G5, 2.5 GHz; two central processing units), using the Conformational Analyzer with Molecular Dynamics and Sampling (CAMDAS) 2.1 program (27). Ten molecular dynamic (MD) calculations were simultaneously performed using different initial structures. Each of the MD calculations was carried out for 1 ns with an integral time step of 1 fs. The lengths of the covalent bonds were fixed. The temperature of the system was maintained at 1,200 K to enhance the sampling efficiency. Conformers were sampled every 100 steps, and then each conformer was minimized until the root mean square of the gradients of the potential energy was below 0.001 kcal mol^{-1} $Å^{-1}$. All conformations were clustered with torsion angles of heavy atoms using a threshold of ±30°. The Merck Molecular Force Field 94s was used to evaluate the potential energy surface of the molecule (28, 29). The dielectric constant was 80, but no cut-off distance for non-bonded interactions was used. Because of the low probability of the existence of conformers with higher energies, the conformers within 15 kcal mol^{-1} of the minimum energy of the molecule were adopted for superposition.

Molecular Modeling of the Arf1-AMF-26-Sec7 Domain Complex—To obtain the initial structure of the Arf1-AMF-26-Sec7 domain complex, the sampled conformers of AMF-26 were superposed onto BFA in the X-ray structure of the Arf-BFA-Sec7 domain complex (PDB code 1r8q) (8) using the parallel version of the SUPERPOSE program (30). This superposes two molecules based on the physicochemical properties of the atomic groups, which is useful for estimating the binding conformation of a molecule by distinguishing it from the many conformations that are generated by CAMDAS. The program considers five types of physicochemical property: hydrophobic (HP), aromatic (AR), hydrogen-bond donors (HD), hydrogen-bond acceptors (HA), and hydrogen-bond donors/acceptors (DA). Each type is represented as a sphere with a predefined radius (1.0 or 0.5 Å) and is assigned to a functional group in a molecule (Fig. 4, *A* and *B*). After molecular superposition, the matching spheres were scored using the scoring matrix (supplemental Table S1). One AMF-26 conformation was chosen as the binding conformation based on the scores and the overlapped molecular volumes (Fig. 4*C*). The superposition calculations were performed using 28 nodes of a Dell PowerEdge 1950III (Intel Quad Core Xeon X5460; 3.16 GHz; 56 central processing units in total). The overlapped molecular volumes were calculated by SYBYL 7.3 (Tripos Inc., St. Louis, MO) on an Hewlett Packard work station xw8200 (Intel Xeon; 3.60 GHz; 2 central processing units).

To relieve the steric hindrances, the coordinates of AMF-26 and of the residues within 4 Å from AMF-26 were optimized to reduce the root mean square of the gradients of potential energy below 0.05 kcal mol^{-1} $Å^{-1}$ using SYBYL. The simplex minimization method before the conjugate-gradient minimization procedure was used. The Tripos force field was employed for the molecular energy calculation. The AMBER 4.1 charges (31) were used as the atomic charges for the proteins and the Gasteiger-Hückel charges (32–35) were used as the charges for AMF-26. The cut-off distance for the non-bonded interactions was 8 Å. The distance-dependent dielectric constant of 4r was used. The initial positions of the missing atoms in the crystal structure were generated by the SYBYL.

Molecular Dynamics Simulation for Model Refinement—To refine the model of the Arf1-AMF-26-Sec7 domain complex, AMBER 9 (36) was used for further minimization and MD simulations on 7 nodes of an Appro 1122Hi (AMD Opteron 248; 2.20 GHz; 14 central processing units in total). The ff99 (37) and gaff (38) force fields were used for the proteins and AMF-26, respectively. The partial charges for AMF-26 were derived from the restraint electrostatic potential method (39) using an *ab initio* calculation at the HF/6–31G* level using Gaussian 03 (40). The complex was solvated in a box of 34616 TIP3P (41) water molecules. Six K^+ ions were added to neutralize the system. The system was minimized until the root mean square of the gradients of potential energy was below 0.005 kcal mol^{-1} $Å^{-1}$. The 3.5-ns MD simulation was carried out at constant pressure (1 atm) and temperature (310 K), under periodic boundary conditions, and with particle-mesh Ewald treatment (42) of electrostatics. SHAKE (43) was applied to all bonds involving hydrogen, and a time step of 1 fs was used. An 8-Å cutoff was used for the non-bonded interactions.

Immunofluorescence Microscopy—After being cultured in a 24-well glass bottom plate for 48 h, cells were treated with chemicals for various periods of time (as indicated in the relevant figure). Cells were washed with PBS, fixed with cold 3.8% paraformaldehyde in PBS (Wako Pure Chemical Industries, Osaka, Japan) for 20 min, and then washed and permeabilized with 0.4% Triton X-100 (Sigma) in PBS for 10 min at room temperature. Cells were incubated in blocking buffer containing 1% BSA and 2% normal goat serum (Dako, Glostrup, Denmark) for 30 min before overnight incubation at 4 °C with primary antibodies diluted in blocking buffer. After being washed, cells were incubated for 1 h with secondary antibodies. Cells were then washed, stained with DAPI (Molecular Probes), and mounted with fluorescent

mounting medium (Dako). The immunostained cells were imaged using a fluorescent microscope IX81 (Olympus Corp., Tokyo, Japan) with a ×100 oil, NA 1.40 objective or with a ×40, NA 0.95 objective, and MetaMorph Software (Molecular Devices, Sunnyvale, CA).

Transferrin Recycling Assay—Transferrin recycling was monitored by modification of a previously published assay (44). 6×10^4 cells were incubated in 24-well glass bottom plates for 48 h, and then in serum-free medium for 3 h to deplete endogenous transferrin. After incubation with 20 μg/ml of Alexa Fluor 488-tagged transferrin (Molecular Probes) in PBBS for 1 h, cells were treated with chemicals for 1 h. Cells were then fixed with 3.8% paraformaldehyde in PBS for 20 min at RT, washed with PBS containing 0.1% 1,4-diazabicyclo[2.2.2]octane (DABCO, Sigma), and mounted with fluorescent mounting medium (Dako).

Flow Cytometry—Cells were harvested, washed with ice-cold PBS, and fixed in 70% ethanol. Cells were then washed twice with ice-cold PBS again, treated with RNase A (500 μg/ml; Sigma) at 37 °C for 1 h, and stained with propidium iodide (25 μg/ml; Sigma). The DNA content of the cells was analyzed with a flow cytometer (FACSCalibur, BD Biosciences).

Animal Experiments—Antitumor effect of AMF-26 was tested *in vivo* against human BSY-1 xenografts in mice. Animal care and treatment was performed in accordance with the guidelines of the Animal Use and Care Committee of the Japanese Foundation for Cancer Research, and conformed to the NIH Guide for the Care and Use of Laboratory Animals. Female nude mice with BALB/c genetic backgrounds were purchased from Charles River Japan, Inc. (Yokohama, Japan), maintained under specific pathogen-free conditions, and provided with sterile food and water *ad libitum*. Each nude mouse was subcutaneously inoculated with the generated tumor fragment of size 3 × 3 × 3 mm. When the tumors reached a volume of 100–300 mm^3, animals were randomly divided into control and AMF-26 groups (each group containing five mice) and daily administration of AMF-26 was then started (day 0). We examined the toxic dose of AMF-26 at a single oral administration. The maximum tolerable dose turned out to be 100 mg/kg of body weight. The experimental group of mice was orally administered a given dose of AMF-26 (83 or 100 mg/kg of body weight) on a daily basis from day 0 to 5. The control group of mice was orally administered with 0.05% Cremophor EL (Sigma) instead of AMF-26. Tumor volume of the tumor-bearing mice was measured as described previously (22). The length (L) and width (W) of the subcutaneous tumor mass of live mice were measured using calipers. Tumor weight was calculated as tumor weight = $(L \times W^2)/2$. To assess toxicity, the body weights of the tumor-bearing mice were measured.

Statistical Analysis—Pearson correlation coefficients were calculated for the COMPARE analysis and statistical correlation. The two-sided Mann-Whitney *U* test was used to assess the statistical significance of the antitumor efficacy of AMF-26 in relative tumor growth ratio on days 3, 7, 11, 14, 17, and 21. The number of samples is indicated in the description of each experiment. All statistical tests were two-sided.

RESULTS

Identification of AMF-26 as a Possible Arf1-ArfGEF Inhibitor by COMPARE Analysis—The JFCR39 panel is a powerful tool for the *in silico* screening of compounds with specific pharmacological activities but with different chemical structures. Seed compounds with desirable pharmacological activities can be used to extract candidates with a similar mode of action in the data base by COMPARE analysis. The data base of our cell line panel holds information on 4,000 compounds, including anticancer drugs and known inhibitors of various biological pathways. Employing this protocol, JFCR39 has been successful in identifying several new anticancer agents, such as a new telomerase inhibitor (FJ5002) (45), an inhibitor of topoisomerase I and II (MS-247) (19), and a novel phosphatidylinositol 3-kinase inhibitor (ZSTK474) (22, 46, 47). For instance, the novel PI3K inhibitor ZSTK474 was structurally different from the known PI3K inhibitor LY294002, although their respective fingerprints were similar. We therefore reasoned that COMPARE analysis would be a suitable method for screening structurally diverse compounds to identify those with a similar mode of action to BFA.

When BFA was used as a seed in COMPARE analysis, AMF-26 was identified to be the compound with a highest correlation coefficient ($r = 0.831$) in the data base based on the fingerprint profile. AMF-26 was the only compound whose *r* value was higher than 0.8 of 4,000 compounds. As shown in Fig. 1*C*, the fingerprint of AMF-26 was similar to that of BFA, which suggested that AMF-26 has a similar biological mode of action to BFA. The mean logarithm of GI_{50} for AMF-26 was −7.33 (at 47 nM), which is comparable with that of BFA (−7.37 at 43 nM). These results indicated that AMF-26 possesses strong growth inhibitory activity as well as that of BFA.

Disassembly of the Golgi Apparatus Caused by AMF-26—COMPARE analysis indicated that AMF-26, like BFA, may be a Golgi disruptor. Therefore, we first examined whether AMF-26 induces Golgi disassembly by immunofluorescence staining with a monoclonal antibody to Golgi brefeldin A-resistant guanine nucleotide exchange factor 1 (GBF1). GBF1 is localized to the *cis*-Golgi apparatus and plays a role in vesicular trafficking by activating Arf1 (48). In control cells, GBF1 was observed in the perinuclear region, forming a ribbon-like structure (Fig. 2*A*). However, addition of BFA caused a rapid release of GBF1 into the cytoplasm (Fig. 2*B*). These results were in agreement with previously published reports (48). When the cells were treated with AMF-26, GBF1 was observed to be dispersed from the perinuclear region throughout the cytoplasm (Fig. 2*C*), which indicated that AMF-26 disrupted the Golgi apparatus. Moreover, this observation was confirmed by live imaging using the MDA-MB-435 stably expressing GFP-conjugated clathrin light chain a (CLCa) cells (supplemental Video S1, *A–C*). In MDA-MB-435/GFP-CLCa cells, the intensity of fluorescence signals of GFP-CLCa were periodically increased and decreased at the TGN, suggesting that the formation of clathrin-coated pits occurs synchronously and periodically at the TGN (23). Disruption of the Golgi apparatus was concurrent with the disappearance of GFP-CLCa signals suggesting that CLCa was affected by AMF-26. Next, we examined whether the

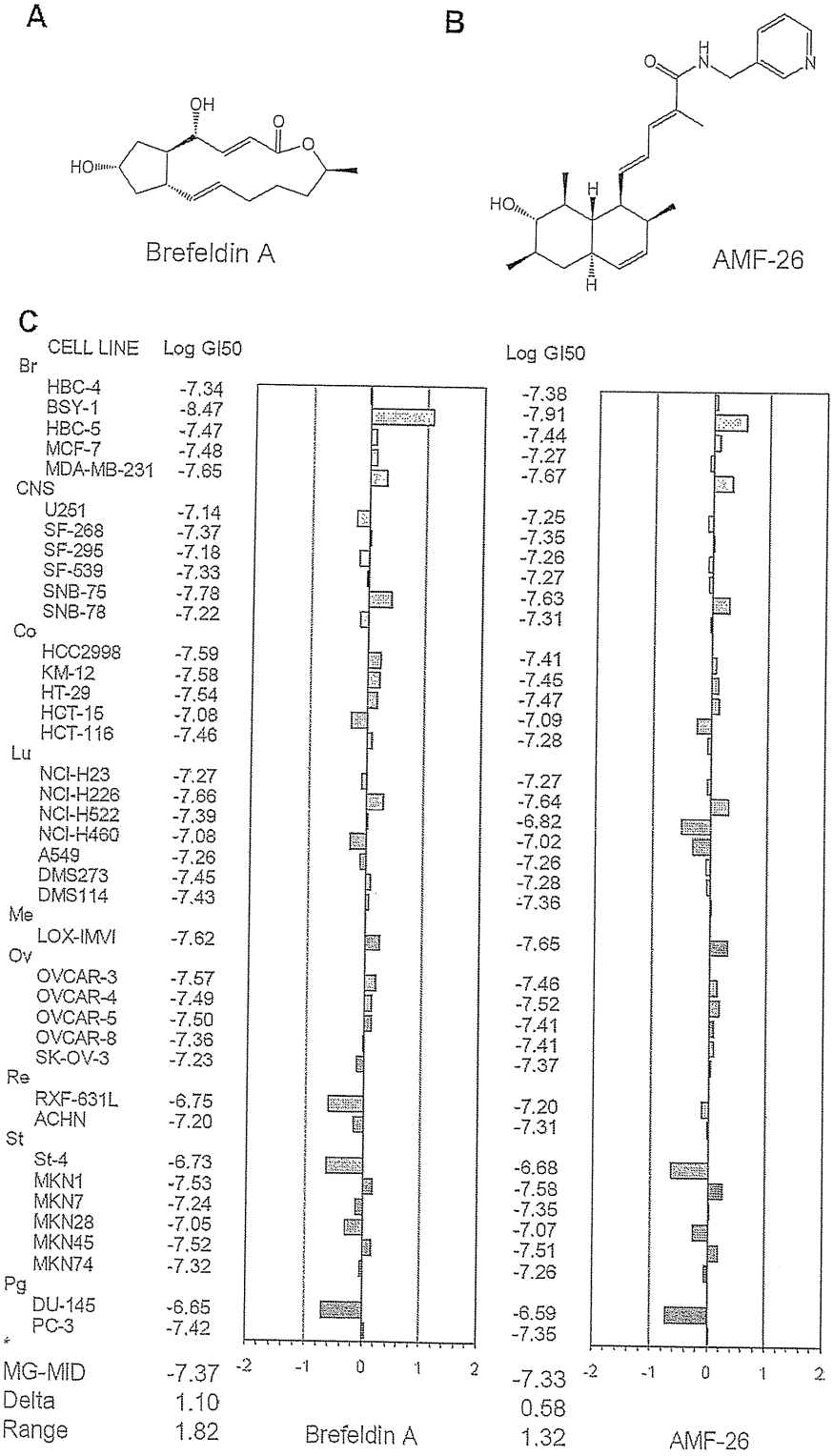

FIGURE 1. **Discovery of AMF-26 as a potent Golgi disruptor.** Chemical structure of (*A*) BFA and (*B*) AMF-26. *C*, growth inhibition against a panel of 39 human cancer cell lines. The mean graph was produced by computer processing of the 50% growth inhibition (GI_{50}) values as described under "Experimental Procedures." Logarithm of the GI_{50} value for each cell line is indicated. In the plot, columns to the *right* of zero indicate sensitivity of the cell line to the compound, and columns to the *left* indicate resistance to the compound. The *x* axis represents the logarithm of difference between the mean of GI_{50} values for 39 cell lines and the GI_{50} value for each cell line in the JFCR39 panel. The mean graph of AMF-26 (*right column*) is very similar to that of BFA (*left column*) (Pearson correlation coefficients; $r = 0.831$). MG-MID, the mean of log GI_{50} values for 39 cell lines; *Delta*, the logarithm of difference between the MG-MID and the log GI_{50} of the most sensitive cell line; *Range*, the logarithm of difference between the log GI_{50} of the most resistant cell line and the log GI_{50} of the most sensitive cell line. One scale represents one logarithm difference. Quantification of the GI_{50} value was represented as the mean of four different experiments. *Br*, breast; *CNS*, central nervous system; *Co*, colon; *Lu*, lung; *Me*, melanoma; *Ov*, ovarian; *Re*, renal; *St*, stomach; *xPg*, prostate.